TABLE OF CONTENTS

1 INTRODUCTION

Glioblastoma multiforme is the most malignant of the astrocytic gliomas and constitutes the most common malignant primary brain tumor (1). Even though glioblastoma multiforme is a quite rare tumor (2), it remains significant due to the median survival time being only 12-15 months from the time of diagnosis (3). The main reasons for the poor prognosis of glioblastoma multiforme are the late stage of diagnosis combined with lack of efficacy of currently available therapies (4, 5). Significant progress in the understanding of cancer biology during the last decades has prompted extensive research within novel classes of anticancer drugs, exploiting molecular differences between tumor cells and cells of healthy tissues (6). Overall, two different strategies have been employed to induce specific cancer cell toxicity, while sparing healthy tissues; 1) targeting of drugs directly to the cancer cells (7, 8), and 2) targeting of drugs to the tumor vasculature (9-11). The first strategy exploits molecular aberrations of cancer cells for specific targeting of drugs, whereas the second approach target abnormalities of the tumor vasculature to reduce the blood supply and inhibit tumor growth. Numerous of targeted therapies are currently in development and several molecular targeted drugs, aimed at interfering with oncogenic cancer cell signaling or angiogenic tumor endothelial cell signaling, have already progressed into the clinical setting. However, the clinical results have largely been disappointing, demonstrating lack of efficiency and resistance development in glioblastoma multiforme patients (6, 7).

Targeted drug carriers are another class of drugs that can be targeted to both cancer cells and the tumor vasculature. However, they are still confined to the early stages of development, but accumulating preclinical evidence demonstrates promising in vivo anticancer effects. (8, 12) One type of targeted drug carriers is the liposomal drug carrier system, which confer some advantages compared to other common drug carriers, e.g. the potential for transporting a wide variety of drugs at a high load per single liposome. Liposomal systems have proven successful for separate targeting of cancer cells and tumor endothelial cells, however both approaches display distinct advantages and disadvantages. (13) A recent development within liposomal cancer therapy combines several types of liposomes directed to different targets or uses multitargeted liposomes, in order to achieve a synergistic targeting effect (14, 15). This strategy could indeed prove advantageous for simultaneous targeting of cancer cells and tumor endothelium in glioblastoma multiforme, in order to benefit from the advantages of the two separate targeting strategies and minimize their disadvantages.

The basic components of the individual liposome and its overall structure are the main determinants of its in vitro and in vivo behavior (16), and therefore great attention must be paid to the specific application, when choosing a liposomal system. Numerous techniques have been developed for the preparation of liposomes and subsequent conjugation with targeting agents (17) . A recently developed approach involves post insertion of lipid micelles conjugated with antibody into preformed liposomes, inducing stable attachment of antibodies to the liposomal surface (18). Traditionally, functional groups for reaction with antibodies have been included in the lipid mixture used for preparation of liposomes, orienting the functional groups randomly in the two leaflets of the liposomal bilayer membrane, but only functional groups protruding on the surface of the liposome will be available for conjugation (13). Using the micelle post insertion technique circumvents this problem, since the functional groups are incorporated into the liposomal membrane after antibody conjugation.

The focus of this thesis is the investigation of liposomes as a possible drug carrier system for targeting cancer cells and tumor endothelial cells of glioblastoma multiforme. In order to address this subject, a suitable animal model for testing in vivo targeting properties of the liposomes as well as a

reproducible protocol for preparation of liposomes are needed. Thus, the three primary aims of this thesis are:

1. Establishment and characterization of an intracranial in vivo model of human glioblastoma multiforme.
2. Development of a protocol for preparation of immunoliposomes using the micelle post insertion technique to attach antibodies.
3. Proof of principle that immunoliposomes specifically can target cancer cells and tumor endothelial cells in the chosen model of human glioblastoma multiforme.

2 BACKGROUND

2.1 Glioblastoma Multiforme

Gliomas denote the most frequent cancer of the central nervous system (CNS), accounting for about 80 % of all malignant primary brain and CNS tumors (1). Gliomas are defined as tumors derived from glial cells and include tumors of astrocytic, oligodendrial, ependymal, or mixed origin. Based on histological appearance, the World Health Organization (WHO) classifies the different types of gliomas into prognostic grades ranging from I to IV. (4) The most malignant astrocytic glioma, glioblastoma multiforme (WHO grade IV), constitutes more than 50 % of all gliomas and is the most common malignant primary brain tumor (1). Even though glioblastoma multiforme is a quite rare tumor with a global incidence rate of only 3.17 per 100,000 (2), it significantly impacts the life of the affected patients due to its poor prognosis with a median survival time of only 12-15 months from the time of diagnosis (3).

2.1.1 Epidemiologic Features

Glioblastoma multiforme may present itself at any age, but typically affects adults, with increasing incidence until aged 85 and above. The median age at diagnosis is 64 years, with more than 80 % of diagnosed glioblastoma patients being older than 55 years and only 1 % younger than 20 years (19). Males are more commonly affected by glioblastoma multiforme, with an incidence rate almost 1.6 times higher than in females (1). The glioma incidence is generally higher in the Western world compared to less developed countries (20). The major reason is probably under-ascertainment of the glioma incidence in developing countries due to limited access to health care, variations in diagnostic practices, and incomplete reporting of glioma cases (21, 22). However, some reports also indicate that ethnic differences in glioma susceptibility may exist. For example, in the United States glioblastoma multiforme is more frequent in Caucasians than in people of African and Asian descent (1). A 1-2 % annual increase in the total brain tumor incidence occurred through the 1980s and 1990s, which primarily is thought to reflect the improved clinical diagnosis of neurological diseases after introduction of high-resolution neuroimaging in the early 1980es. However, a true rise in incidence for at least some types of brain tumors cannot be excluded, but such evidence are yet to be demonstrated for glioblastoma multiforme. (21)

For the majority of gliomas no underlying carcinogenetic causes can be identified. So far, the only established environmental risk factor reported is exposure to high-dose, ionizing radiation (21, 23). Several epidemiological studies have also demonstrated an association between increased glioma risk and other environmental factors, including severe head injury, dietary risk factors, occupational risk factors, and exposure to electromagnetic fields. However, the data regarding the suggested risk factors remain inconclusive, since other studies failed to identify any link to glioma development. (21, 22, 24) More consistent reports suggest a protective effect of allergic diseases and infections, indicating that immune surveillance mechanisms stimulated by these conditions inhibit glioma development (21, 23).

Genetic predisposition has been observed in 5-10 % of glioma cases (22). Rare genetic syndromes associated with an increased risk of glioma such as neurofibromatosis 1 and 2, tuberous sclerosis, retinoblastoma (RB) 1, Li-Fraumeni syndrome, Turcot's syndrome, and multiple harmatoma only account for few cases (21, 23). Gliomas have also been observed to run in families, not affected by the listed syndromes, but implicated susceptibility genes remains yet to be identified. In addition, the causal relationship between glioma and common polymorphisms in genes involved in detoxification of

carcinogens, cell cycle regulation, and DNA repair mechanisms, have been investigated only to reveal vague or no association. (22, 23)

2.1.2 Pathological Features

Glioblastoma multiforme lesions are typical large at the time of diagnosis and may occupy much of a brain lobe. The lesions are often located in the subcortical white matter of the cerebral hemispheres and frequently extend across the border of the frontal lobe into the temporal lobe. Tumor infiltration has often progressed into the adjacent cortex and through the corpus callosum into the contralateral hemisphere. (4).

The tumor mass of glioblastoma multiforme is characterized by being poorly delineated and having a high degree of regional heterogeneity. Highly proliferating cancer cells are usually found in the peripheral, hypercellular zone of the tumor, whereas the central tumor area mainly consists of necrotic tissue, comprising up to 80 % of the total tumor mass. Histopathologically, the lesions typically exhibit cellular hyperplasia in peripheral zones harboring cancer cells with atypical nuclei, increased mitotic activity, cellular pleomorphism and poor stages of differentiation. A diagnostic feature of glioblastoma multiforme is the presence of areas with vascular hyperplasia, necrosis or both in the tumor tissue. Another hallmark of glioblastoma multiforme is rapid invasion of the surrounding brain tissue, especially along myelinated brain structures such as the corpus callosum or within perivascular spaces. Infiltrating tumor cells are dispersed within the normal brain tissue surrounding the contrast-enhancing tumor border at high-resolution scans. These satellite cancer cells are thought to be the origin of local tumor recurrence after therapy, since the infiltrating cells escape surgical resection and high-dose radiotherapy of the primary tumor mass. Despite the highly infiltrative nature of glioblastoma multiforme, it tends to invade neither the subarachnoidal space nor the vessel lumen, and therefore distant metastases are rarely found, both within and outside the CNS. (4).

Glioblastoma multiforme lesions most commonly occur as primary glioblastoma without clinical evidence of a preceding lesion within the CNS (25, 26). Only about 5 % of glioblastoma multiforme cases progress from lower grade astrocytomas into secondary glioblastoma (25). The time to progression is highly variable, with time intervals ranging from less than 1 to more than 5 years before occurrence of glioblastoma multiforme. Primary lesions typically affect older patients with a mean age of 62 years at diagnosis, whereas secondary glioblastoma in contrast develop in younger patients with a mean age of 45. (27) Phenotypically, primary and secondary glioblastoma are indistinguishable. However, the two glioblastoma multiforme subtypes display distinct genetic abnormalities, suggesting that their malignant transformation occurs through different genetic pathways. Primary glioblastoma in adults is associated with epidermal growth factor receptor (EGFR) overexpression and mutation, loss of heterozygosity (LOH) of chromosome 10q, mutation of the phosphatase and tensin homology (PTEN) gene, and deletion of the p16 gene. Mutations in the p53 gene, LOH of chromosome 10q, and abnormalities in the pathway regulating the tumor suppressor RB are frequently found in secondary glioblastoma multiforme. Overall, these genetic alterations in both primary and secondary glioblastoma multiforme result in overactivation of several mitogenic signaling pathways that ultimately leads to uncontrollable growth of the affected cells. (25, 26)

The cellular origin of glioblastoma multiforme is a subject of ongoing investigation. Traditionally, it was believed that glioblastoma multiforme arose from mature astrocytes, and that expression of progenitor cell markers was the result of de-differentiation during the process of malignant transformation (4). However, recent research suggests that the tumors may stem from malignant transformation of neural stem cells or related progenitor cells (28). In agreement with this theory, cancer cells

with stem cell-like properties have been isolated from glioblastoma tumors and cell lines. These so-called cancer stem cells only account for a small fraction of the tumor, but exhibit classical stem cell properties such as an extensive proliferative potential, self-renewal, and multipotency. Furthermore, the isolated cancer stem cells display pronounced tumorigenic behavior when implanted into immunocomprised mice, giving rise to tumors mimicking the phenotype and recapitulating all the different cell types of parent tumors. Cancer stem cells may therefore be the driving force of glioblastoma multiforme growth through their unlimited growth potential. (29) Accumulating evidence suggest that the cancer stem cells may represent descendents of neural stem cells or related progenitor cells that suffered the initial carcinogenic insult, but still the possibility of de-differentiation of more mature astrocytes have not been disproved (28). Thus, distinct proof of the cellular origin of glioblastoma multiforme as well as their inherent cancer stem cells still remains to be found.

2.1.3 The Process of Neovascularization

All solid tumors depend on formation of new blood vessels for nutritional support of their growth beyond 1 mm^3 (30). Glioblastoma multiforme is one of the most vascularized human tumors, and depends on several processes for vascularization, the three most important being vessel co-option, vasculogenesis, and angiogenesis (4). Vessel co-option is the adoption of pre-existing vessels within the normal brain tissue by perivascular migrating tumor cells at the periphery of the tumor. In addition, the cancer cells secrete signaling molecules that stimulate vasculogenesis through recruitment of circulating bone-marrow derived cells and their subsequent incorporation into new blood vessels at the tumor site. (31) Angiogenesis is the sprouting of normal vessels into the tumor area, mediated by endothelial cell proliferation and migration, together with concurrent remodeling of the perivascular extracellular matrix (32). The process of angiogenesis occurs in response to proangiogenic growth factors secreted either by cancer cells or stromal cells of the tumor. In virtually all gliomas, vascular endothelial growth factor-A (VEGF-A) comprise the major proangiogenic growth factor. Hypoxia strongly stimulates VEGF-A expression in gliomas, and upon secretion VEGF-A induce vascular permeability as well as endothelial cell proliferation and migration. Other important proangiogenic growth factors include fibroblastic growth factor (FGF), the angiopoietins (Ang 1 and Ang 2), and platelet-derived growth factor (PDGF). (31, 32)

The neoangiogenic blood vessels formed in the periphery of glioblastoma multiforme lesions are both structurally and functionally abnormal. The tumor vessels are tortuous, disorganized, and have a significantly larger diameter than vessels of the normal brain. In addition, the vessel wall is characterized by abnormalties in endothelial cell function, pericyte coverage, and expression of basement membrane proteins. (31) The disordered vasculature leads to an increased resistance to blood flow, reducing the overall perfusion and distributing blood heterogeneously within the tumor (31, 33). The tumor vessels are also highly permeable to macromolecules of the blood as compared to the restricted vascular transport across the blood-brain-barrier of normal brain vessels. However, the severity of blood-brain barrier compromise in the tumor area is known to vary both temporally and spatially. (33) The increased permeability of the vasculature leads to accumulation of fluid and plasma proteins in the tumor and surrounding brain tissue. Due to the lack of lymphatics, extravasated fluid accumulates within the tumor and results in an increased interstitial pressure, leading to vasogenic brain edema and increased intracerebral pressure. (31) Furthermore, the insufficient and heterogeneous perfusion of the tumor results in regional hypoxia and acidosis, reducing sensitivity of the cancer cells to radiation therapy. The heterogeneous blood supply combined with a high interstitial pressure also disturbs the delivery of blood-borne therapeutics to the cancer cells of glioblastoma multiforme. (33)

2.1.4 Clinical Presentation and Diagnosis

Symptoms of glioblastoma multiforme usually present late in the course of the disease, and typically the first clinical signs are those of raised intracranial pressure, e.g. headache, nausea and/or vomiting, and papilledema. Other frequent symptoms include non-specific neurological symptoms, such as focal neurological deficits, personality changes, confusion, memory loss, and tension headaches. In addition, one third of patients experience at least one epileptic seizure. (4, 5) Presentation of persistent neurological symptoms prompts magnetic resonance imaging or computed tomography scanning of the brain, and detection of a heterogeneously enhancing mass with surrounding edema suggests the diagnosis of malignant glioma. Irregular enhancement and extensive peritumoral edema indicate the lesion being glioblastoma multiforme rather than anaplastic glioma, but the diagnosis can only be histopathologically confirmed at surgical debulking of the tumor mass. (5)

2.1.5 Conventional Treatment

Standard therapy for newly diagnosed glioblastoma multiforme consists of surgery followed by radiotherapy with concomitant and adjuvant chemotherapy. Complete surgical resection of the tumor is not possible due to its highly infiltrative growth, but surgical debulking is performed to maximally reduce tumor size. Subsequent postoperative radiotherapy is delivered by partial-field external beam-irradiation, targeting brain tissue at a 2-3 cm margin around the operative cavity. (5) The main chemotherapeutic agent used for treatment of glioblastoma multiforme is temozolomide, an oral alkylating agent with a reasonable penetration of the normal blood-brain barrier (34). Despite best available treatment, tumor recurrence is observed in basically all patients diagnosed with glioblastoma multiforme, and the mean time to progression is only 6.9 months from the time of diagnosis (3). Therapy of recurrent glioblastoma consists of tumor reoperation if symptoms of the mass effect are evident, radiotherapy, various combinations of conventional chemotherapeutics, and experimental therapies (35, 36). Common side effects accompanying glioblastoma multiforme therapy include toxicity to adjacent brain structures, toxicity to proliferating cells of non-neuronal tissues, and unwanted long-term effects like cognitive deficits and epilepsy due to neuronal damage (5).

Despite recent progress in the therapeutic management of glioblastoma multiforme, the five year patient survival is still less than 5 %, and the disease is basically incurable due to the high rate of recurrence (1). The reason for this is both the late stage of the disease at diagnosis, and the inability of available therapy to efficiently eradicate all glioblastoma cells. Advances in glioblastoma multiforme therapy are clearly required to improve the patient survival together with a reduction in side effects of medical treatment. Recent advances in understanding glioma biology hold promises for development of therapeutics that specifically target the tumor compartment, and multiple experimental therapies based on this approach are currently in development (6).

2.2 Targeted Cancer Therapy

According to the original “magic bullet theory”, presented by Paul Ehrlich more than 100 years ago, cancer cells can be specifically targeted by directing drugs to molecular targets exclusively found in malignant cells.

Identification of such drugs would result in selective cancer cell toxicity, while sparing normal tissues. (37) Thus, the “magic bullet theory” has long fascinated researchers and inspired them to search for tumor specific molecules as well as drugs that are able to target these molecules. In general, the conducted research has focused on two different drug targeting strategies in a variety of solid tumors; 1) targeting drugs directly to the cancer cells (7, 8), or 2) targeting drugs to the tumor vascula-

ture (9-11). The first strategy promotes specific interaction of the drug with the cancer cells to exert its effects, whereas targeting drugs to tumor endothelial cells aim at regression of the tumor vasculature and subsequent starvation of the cancer cells.

Independent of the targeting strategy, the chosen target molecule must be effectively targeted by the applied drug. First of all, the target must be highly specific for the tumor in order to achieve selective targeting. If the target molecule is expressed by cells of other tissues, this could result in off-target side effects and toxicities. The target molecule must also be abundantly expressed in the tumor area to ensure sufficient interaction between drug and target cell. Furthermore, a stable expression of the target molecule is of great importance, preventing down-regulation of the target molecule during malignant progression of the tumor and during treatment with targeted therapeutics. Unfortunately, it has proven difficult to identify molecular targets that meet all of the listed criteria, neither for cancer cells nor for tumor endothelial cells. (7, 13, 38, 39) Despite difficulties in identification of optimal targets, extensive research in targeted cancer therapies during the last decades have generated a variety of targeting strategies and agents that have potential for use in the clinical therapy of glioblastoma multiforme.

2.2.1 Targeting of the Cancer Cells

Targeting cytotoxic drugs directly to glioblastoma cells has been proposed as a strategy to achieve a more pronounced antitumor effect and fewer side effects. Compared to conventional chemotherapy, targeted drugs will have a selective cytotoxic action on cancer cells, while having no or only a modest effect on normal cells. A higher accumulation of the therapeutic drug in the tumor compartment can also be achieved, either by promotion of the cellular uptake through binding of the drug to the target molecule (e.g. an internalizing cell surface receptor) or by administration of high drug doses, which only is possible due to the few off-target side effects. (6, 8) However, an obstacle for direct targeting of cancer cells is that the drug of choice needs to penetrate into the tumor to exert its therapeutic effects. The high intratumoral interstitial pressure and the only partially disrupted blood-brain barrier in glioblastoma multiforme lesions act as barriers (31, 33), reducing the tumoral delivery of blood-borne tumor-targeted drugs (7, 13).

Drugs targeting cancer cells directly can be divided into two main groups based on the mechanism of interaction with their target. The first group, known as molecular targeted drugs, aim at interfering with intracellular signaling pathways, which are overactivated in glioblastoma and drive cellular proliferation, survival and invasion (6, 40). Molecular targeted drugs exert their anticancer effects by binding directly to a target molecule involved in cellular signaling and thereby inhibiting the normal functions of this molecule (6, 7, 41). The second group of drugs targeting cancer cells is in general encompassed by various types of drug carriers. Here, the carrier transporting the cytotoxic drug prevents interaction of the drug with healthy cells, and modification of the drug carrier with a ligand or antibody directs the drug carrier towards a specific cancer cell surface molecule. The main objective of the target molecule is to establish contact between the drug and the cancer cell, and possibly facilitate uptake of the drug into the intracellular compartment, where it exerts its effects. (12)

Identification of mitogenic signal transduction pathways frequently overactivated in glioblastoma has lead to development of molecular targeted drugs for treatment of glioblastoma multiforme. Examples include different types of EGFR inhibitors, such as cetuximab (Erbitux), a monoclonal antibody against EGFR which blocks the binding of EGF and prevents receptor activation (42), and the EGFR tyrosine kinase inhibitors gefitinib (Iressa) and erlotinib (Tarceva) which inhibit activation of the receptor-coupled tyrosine kinase (7). Other targets are intracellular signaling molecules acting

downstream of EGFR and other growth factor receptors (25, 26). Drugs targeting such molecules are the farnesyltransferase inhibitor tipifarnib (Zarnestra), and the mammalian target of rapamycin (mTOR) inhibitor temsirolimus (Torisel) (6, 7). Overall, the antitumor effects of molecular targeted drugs investigated as monotherapy in glioblastoma multiforme have been largely disappointing and have not demonstrated survival benefits compared to standard therapy. A major problem that limits the therapeutic efficacy of molecular targeted drugs is their poor intratumoral accumulation due to the blood-brain barrier and the high interstitial pressure, restricting the amount of drug that can accumulate in the tumor and exert its effect on the cancer cells. This is especially true for the large monoclonal antibodies, whereas the tyrosine kinase inhibitors have an advantage due to their small molecular weight. (6, 7) Various strategies to improve the efficacy of molecular targeted drugs are currently being investigated in clinical trials. They include the combination of molecular targeted drugs with conventional therapy or other targeted drugs, selection of patients on the basis of biomarkers, and development of new, more powerful drugs against the same or newly discovered targets. (7, 41)

Numerous targeted drug carriers have been studied preclinically in animal models of glioblastoma multiforme, however few have progressed to clinical trials. The investigated drug carriers include protein toxins and doxorubicin-liposomes targeted primarily to the transferrin receptor or interleukin receptors, overexpressed on the surface of glioblastoma cells (43-45). Targeted protein toxins are the only tumor-directed drug carriers that are currently in clinical trials for glioblastoma multiforme. These large drugs must be delivered locally into the tumor through an invasive procedure, known as convection-enhanced delivery, based on infusion of the drug through catheters inserted in the brain. (46-49) The targeted protein toxins consist of a bacterial toxin that have been mutated at its cell binding domain to prevent unspecific binding to healthy mammalian cells and then conjugated to a targeting molecule. Examples of protein toxins in clinical trials for glioblastoma multiforme are Tf-CRM107 (TransMID) (46), a modified diphtheria toxin conjugated to transferrin, as well as interleukin-4 PE38KDEL and interleukin-13 PE38QQR (Cintredekin besudotox), two different versions of the pseudomonas exotoxin conjugated to an interleukin (44, 45). Administration of these protein toxins to glioblastoma patients in phase I and II clinical trials has generally demonstrated their safety and some evidence of radiographic responses (46, 47, 50-52).

Targeted liposomes are another type of drug carriers that have been suggested for therapy of glioblastoma multiforme. An advantage of using a liposomal drug carrier system compared to drug- and protein-conjugates is that a large variety of drugs can be encapsulated and a large drug load can be delivered within a single liposome (13). So far, targeted liposomes have only been tested preclinically in animal models of glioblastoma multiforme. Such studies have primarily focused on liposomes containing the chemotherapeutic doxorubicin, since this drug is both a highly potent chemotherapetic and easy to encapsulate efficiently in liposomes (53). Previously, untargeted liposomal doxorubicin has demonstrated an improved toxicity profile and antitumor effects both in patients with glioblastoma multiforme and relevant animal models (54-56). In addition, untargeted doxorubicin liposomes have already been approved for clinical use in therapy of several other cancer types (12). Both untargeted and targeted long-circulating liposomes accumulate passively in tumors after intravenous injection due to the leakiness of newly established tumor vasculature and the lack of lymphatics, known as “the enhanced permeability and retention effect (EPR)” (8, 57). In animal models of glioblastoma multiforme, doxorubicin liposomes have been targeted to the interleukin-13 receptor through conjugation with interleukin-13 (58), while antibodies have been used for directing the liposomes to the EGFR (59) as well as cell surface bound-nucleosomes, originating from apoptotic cancer cells (60). Overall, the

available preclinical data demonstrate superior antitumor activity of targeted formulations of liposomal doxorubicin as compared to untargeted liposomes and unencapsulated drug (58-60).

2.2.2 Targeting of the Tumor Vasculature

Targeting drugs to the tumor vasculature of glioblastoma multiforme is an attractive treatment strategy due to the high degree of vascularization of this tumor and its dependency on new blood vessel formation for nutritional support. Inducing damage to the tumor blood vessels or inhibiting angiogenesis deprives the cancer cells of oxygen and nutrients, while preventing removal of waste products. The resulting hypoxia, starvation of cancer cells, and buildup of waste products eventually leads to cessation of tumor growth and cancer cell necrosis. (61) Targeting the tumor vasculature has some advantages compared to direct targeting of the cancer cells. First of all, blood-borne drugs have easy access to target molecules expressed by tumor endothelial cells without any need to transverse the endothelium (62, 63). In addition, vascular disruption has the potential to exhibit a significant amplification effect, since a single blood vessel might supply a large number of cancer cells (62, 64). With the tumor endothelium being derived from the normal vasculature, it was traditionally thought that tumor endothelial cells displayed a higher degree of genetic stability than cancer cells, thereby reducing the probability for development of drug resistance to vascular targeted therapy (65). However, it is now generally accepted that tumor endothelial cells in fact demonstrate a significantly higher mutation rate than normal endothelial cells, which significantly aid in development of resistance to vascular targeted therapies. Another challenging aspect of targeting the tumor vasculature is the heterogeneous vascular structure and associated molecular profile, varying both spatially and temporally (31). Therefore any applied targeting molecule is unlikely to affect the tumor vasculature evenly, and a combination of vascular targeting drugs might be necessary to achieve a satisfactory effect.

The class of vascular targeting drugs that has received most attention in the management of glioblastoma multiforme is without any doubt the angiogenesis inhibitors. These drugs aim at interfering with formation of new blood vessels and thereby inhibiting tumor growth. The angiogenesis inhibitors are basically molecular targeted drugs directed towards secreted proangiogenic growth factors, their cell surface receptors, or other molecules involved in angiogenesis, such as proteases or cell surface adhesion molecules (9, 10). Another drug class inhibiting blood supply to the tumor is the vascular disrupting agents (VDAs) that cause rapid shutdown of the established tumor vasculature (11, 62, 66). VDAs can be divided into two main groups, i.e. small-molecule and ligand-based VDAs (11). Small-molecule VDAs induce selective damage to tumor endothelial cells by exploiting their structural and molecular abnormalities, such as increased proliferation, vascular permeability, and impaired reliance on the cytoskeleton to maintain cell shape. In contrast, ligand-based VDAs target toxins, procoagulant or proapoptotic molecules to the vasculature through antibody- or peptide-conjugated drug carriers. (11, 38)

The development of angiogenesis inhibitors for cancer therapy has primarily focused on VEGF signaling (10, 61), which is a cornerstone of the angiogenic process in malignant glioma. The angiogenesis inhibitor bevacizumab (Avastin) has already been approved for monotherapy of glioblastoma multiforme after progression on conventional therapy in the USA (10). Bevacizumab is a monoclonal antibody that binds to secreted VEGF-A, preventing it from interacting with VEGFR-2 to exert its proangiogenic effects (61) In addition, several tyrosine kinase inhibitors acting at the intracellular VEGFR-2 coupled tyrosine kinase have gone into clinical trials for therapy of glioblastoma multiforme (10, 61). One example are the pan-VEGFR tyrosine kinase inhibitor cediranib (Recentin) with additional activity against PDGF receptor (PDGFR) and c-Kit (67). Alternatives to VEGF and VEGFR inhibi-

tion currently being evaluated in glioblastoma multiforme patients include the fibroblast growth factor receptor tyrosine kinase inhibitor brivanib, the PDGFR tyrosine kinase inhibitors tandutinib and dasatinib (SPRYCEL), and the αvβ3/αvβ5 integrin inhibitor cilengitide (10, 61). In general, angiogenesis inhibitors have displayed some antitumor activity in glioblastoma multiforme, when administered as monotherapy. Moreover, a synergistic effect has been observed in combination with chemotherapy both preclinically (68) and clinically (69). A key factor of this synergistic effect might be that angiogenesis inhibitors transiently can "normalize" the abnormal tumor vasculature by reducing the high permeability and diameter of the dilated blood vessels. Vessel "normalization" could possibly result in more efficient delivery of conventional chemotherapeutic agents due to a better perfusion of the tumor and decreased tumoral interstitial pressure (70-73). It has also been hypothesized that better perfusion can lead to better oxygenation of cancer cells, resulting in higher sensitivity to radiotherapy (72). Another benefit of the decreased interstitial pressure induced by antiangiogenic therapy is the appertaining reduction of the need for corticosteroid treatment of vasogenic brain edema in the patients, hereby avoiding potentially serious side effects (70, 72). However, the clinical use of antiangiogenic therapy is complicated by fast development of tumor resistance and unresponsiveness to these drugs, primarily due to activation of alternative angiogenic signaling pathways. Furthermore, a significantly more invasive phenotype of glioma cells have been observed in tumors treated with antiangiogenic therapy. (61)

VDAs have not been as extensively investigated in glioblastoma multiforme as in other cancers, and for glioblastoma multiforme only few preclinical studies have been carried out (62). However, in other cancers, especially small-molecule VDAs have shown clinical safety and promising antiproliferative results in clinical trials (11, 62). Flavone acetic acid and its derivative 5,6-dimethylxanthenone-acetic acid constitute some of the most studied small-molecule VDAs (62). Their mechanism of action are based on of the release of tumor necrosis factor α (TNF-α) and other cytokines from the tumor endothelial cells, which leads to increased vascular permeability and hemorrhage, resulting in widespread cancer cell necrosis (74). Only two ligand-targeted VDAs have been investigated in experimental models of glioblastoma multiforme. Both are bacterial toxins conjugated to ligands targeting either the urokinase-type plasminogen activator receptor, expressed by both endothelial cells of the neovasculature and glioma cells, or the VEGFR-2 of the tumor endothelial cells (75, 76). In other experimental in vivo cancer models several other ligand-targeted VDAs have been examined. The VDAs include fusion proteins, immunotoxins, drug-conjugates and immunoliposomes targeted to different de novo expressed membrane proteins on the tumor endothelial cells vasculature, like vascular cell adhesion molecule-1 (VCAM-1) (77-79), integrins (80-85), aminopeptidase N (14, 14, 86, 87), endoglin (88-90), VEGFR-2 (91-95), and extracellular matrix proteins, such as ED-B domain of the glycoprotein fibronectin (96-100). Some of these targets could also have potential for vascular targeting in glioblastoma multiforme. In summary, the potential of applying VDAs in therapy of glioblastoma multiforme largely remains to be elucidated. In preclinical studies of other cancer conditions, the various VDAs have shown little effect as monotherapy (11). A viable rim of cancer cells have been shown to survive at the periphery of the lesion, and it is believed that these cells can serve as a source for tumor regrowth. Because these cancer cells derive oxygen and nutrients from blood vessels in adjacent normal tissue, their good state of oxygenation and high rate of proliferation make them sensitive to radio- and chemotherapy, respectively (11, 38). Enhanced antitumor activity have been demonstrated in experimental in vivo models of glioblastoma multiforme using combined therapy of VDAs with radiotherapy or chemotherapy (11, 38), and this is currently being investigated in various clinical trials.

2.2.3 Combining Targeting of the Cancer Cells and the Tumor Vasculature

Molecular targeted drugs and antiangiogenic drugs, which are the targeted drugs in most advanced development, both suffer from problems with lack of efficacy and resistance development and further optimization of these drugs is needed to achieve the desired effects. The use of targeted drug carriers is an approach that can be applied to targeting of cancer cells directly as well as targeting of the tumor vasculature, and both types of carriers are largely unexplored in glioblastoma multiforme. Targeted liposomes seem to be a good carrier choice, since a large drug load can be transported by a single carrier, and a large variety of drugs can be encapsulated. Furthermore, the development of resistance mechanisms could be prevented by using several types of targeted liposomes, each directed at a different target and possibly containing different therapeutic drugs. An obvious approach could be to target one type of liposomes to the cancer cells and another type to the tumor endothelial cells, in order to benefit from the advantages of both targeting strategies and minimize some of their separate disadvantages.

2.3 Liposomes as a Drug Delivery System

The use of liposomes a drug carrier system were proposed several decades ago and since then it has been one of the most extensively investigated drug carrier systems. Modication of the basic liposome structure and optimization of methods for preparation of liposomes have overcome many of the initial obstacles encountered, when applying liposomes in vivo. Today liposomes can be tailor-made in many aspects to meet the demands needed for a specific in vivo application.

2.3.1 Different Types of Liposomes

Liposomes are lipid bilayer vesicles within the 50-1000 nm range, containing an aqueous core. Unilammellar liposomes consist of a single lipid vesicle with an aqueous core, whereas multilammeller liposomes contain several lipid vesicles inside each other. Lipids can be made from various mixtures of natural and synthetic lipids, however the specific lipid composition is an important determinant of the liposomal in vitro and in vivo characteristics of the liposomes (101). Liposomes are well suited for the use as drug carriers, since they have the ability to transport many different types of drugs at high concentrations. Hydrophilic and amphiphilic drugs can be encapsulated into the aqueous core, whereas hydrophopic drugs can be incorporated into the lipid bilayer. (53)

To control the cellular fate of liposomes, they can be modified with various surface molecules, such as polymer-coatings and targeting agents. Based on such modifications, unilammellar liposomes have been divided into several types. The first liposomes to be investigated were unilammellar liposomes between 100-500 nm without any surface modifications, named conventional liposomes (Figure 1A). Investigating various formulations of conventional liposomes revealed that in vivo circulation time and other pharmacokinetic parameters were closely related to size, lipid composition and charge of these liposomes (53). For example, small liposomes (< 100 nm) containing gel-state phospholipids and cholesterol had a significantly longer circulation time than larger liposomes of the same lipid composition (102). In addition, neutral liposomes were generally found to have a longer circulation time than electrostatically charged liposomes (53). The fast removal of conventional liposomes from the circulation is predominantly caused by a rapid liposomal uptake by the macrophages of the reticuloendothelial system (RES) in the liver and spleen (53). To overcome this problem liposomes coated with linear polyethylene glycol (PEG) molecules was developed, limiting the rapid uptake by the RES and significantly prolonging the half life of circulating liposomes to about 20 hours in mice and rats (103) and up to 45 hours in humans (104). PEG are commonly grafted to the liposomes by modifi-

cation of the PEG molecules with a hydrophobic residue at one end, typically a phospholipid, which then can be incorporated into the bilayer of the liposomal membrane (Figure 1B). As for conventional liposomes, liposome size was also found to be an important factor in liposomal clearance for PEGylated liposomes after intravenous injection (53). Prolonged circulation was especially observed for small liposomes with a size of 70-200 nm and a high degree of homogeneity (105). In contrast, 300-400 nm PEGylated liposomes avoided significant entrapment in the liver, but not of the red pulp and marginal zone of the spleen (106). Thus, the biodistribution pattern of liposomes can significantly be altered by changing their basic structure of both conventional and PEGylated liposomes.

The next step in the development of liposomes as drug carriers involved preparation of liposomes that were conjugated with a targeting ligand. This enabled direction of the liposomes towards specific molecules expressed by the target cell population, promoting close interaction of the liposomes with the target cell and possibly cellular internalization. Two different approaches was investigated for conjugation of liposomes; 1) coupling the targeting ligand directly to the lipid bilayer, which was explored for both conventional and PEGylated liposomes (Figure 1C and D) coupling of the targeting ligand to the distal end of surface grafted PEG-chains of PEGylated liposomes (Figure 1E). (13) The simplest approach is method one and worked well for conjugation of conventional liposomes. However, for conjugation to PEGylated liposomes a major drawback was that the flexible PEG-coat could both prevent interaction of the conjugated ligand with its target, as well as the reaction for conjugation of ligands to reactive groups on the liposomal surface (107, 108). Due to these constraints, methods for coupling ligands to the distal end of PEG-chains were developed, restoring the availability of the conjugated ligand for interaction with its target.

The most commonly used types of targeting ligands used for conjugation to liposomes are antibodies or fragments hereof and peptide ligands (13). When choosing a targeting ligand for liposomal conjugation, it is not only important to ensure that the targeting ligand binds specifically to a target sufficiently expressed by the target cell, but several other considerations must also be taken into account to choose the best type of targeting ligand and chemical method for attaching of the ligand to the liposome.

First of all, conjugating a ligand to the surface of a liposome may increase the rate of liposome uptake by the RES, despite the presence of PEGylation. Next, the immune system might attack the ligand or other parts of ligand-conjugated liposomes and cause an unwanted immune reaction. (13, 109) The extent of antibody development depends both of the type of ligand, e.g. a small peptid or Fv fragment is usually less immunogenic that a complete foreign antibody, and the lipid composition of the liposome (110, 111). Based on these principles, it is understandable why the amount of conjugated ligand must be balanced to establish successful binding to its target, while maintaining a long circulation time. Using liposomes with a lower ligand-density may extend the liposome circulation time and improve the chance of interaction with targets located in tissues with limited blood flow, whereas such liposomes might not bind most efficiently to the same target in vitro compared to liposomes maximally conjugated with ligand.

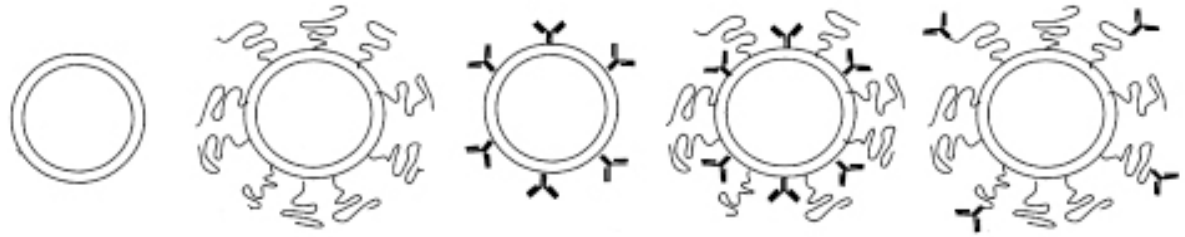

Figure 1: Scematic representation of different types of liposomes. A) Conventional liposome. B) PEGylated liposome. C) Conventional liposome with antibodies conjugated directly to the liposome surface. D) PEGylated liposome with antibodies conjugated directly to the liposome surface. E) PEGylated liposomes with antibodies conjugated to the distal end of PEG-chains. Modified from (112)

2.3.2 In Vivo Properties of Liposomes

The behavior of the various formulations of liposomes has been extensively studied at the cellular level both in vitro and in vivo, as well as at whole organism level in vivo. As mentioned above, the fate of liposomes in vivo is determined by the structure and single components of the liposome, such as size, lipid composition, PEGylation, and the presence of targeting ligands on the surface.

The predominant administration route for liposomes is by intravenous injection, after which the liposomes circulate in the blood. Due to the large size of liposomes the lining of the blood vessels act as a barrier and the liposomes can only extravasate at sites with discontinuous or fenestrated endothelium (53). Both the liver and spleen have fenestrated endothelium, and therefore liposomes not exceeding the size of the fenestrae are prone to accumulate in these organs. However, accumulation of liposomes within these organs has been demonstrated not to depend solely on the size of the liposomes, but also their lipid composition. For example liposomes with a significant larger size than the pore size of the liver fenestrae, but having a high fluidity, were found to accumulate in the liver in a high degree. Accumulation of liposomes in the liver and the spleen promote the interaction with the large quantity of inherent macrophages of the RES, which are the main source of liposome elimination from the body. Depending on the size and lipid composition of the liposomes, liver hepatocytes may also play an important role in removing liposomes from the blood. No convincing evidence have demonstrated a significant uptake of liposomes by other cell types easily accessible from the blood, such as cell of the endothelium or circulating blood cells. (16)

Several theories exist for the mechanisms of liposome removal by the RES, and why PEGylation of the liposomes slow down this process. In the circulation, liposomes of various compositions unspecifically adsorb proteins present in serum, and one theory is that the opsonization of liposomes promotes the clearance by macrophages through receptor-mediated endocytosis by the means of some of the liposome bound proteins (53). Some of the identified proteins that opsonize liposomes include fibronectin, complement factors, β2-glycoprotein, C-reactive protein, and α2-macroglobulin (113-117). After receptor-mediated endocytosis of the liposomes, lysosomal digestion of the liposome membrane releases the liposomal content into the cytoplasm. Several theories have been proposed to explain why PEGylation increase the circulation times of liposomes. One of the most popular views suggests that the PEG-chains act as a steric barrier, preventing macromolecules such as the mentioned opsonins from interacting with the liposomal membrane. Due to the lack of liposome opsonization the rate of macrophage uptake is significantly reduced. (53)

Long-circulating liposomes have a higher probability for encountering their target cells, especially if located in an area with limited blood supply, and a longer circulation also increase the probability of extravasation and accumulation at sites with increased vascular permeability, such as in tu-

mors (16). Increasing the circulation time will increase the number of times a liposome passes through a specific tissue, and thereby increasing the probability of interaction with its target cell or increasing the probability of intratumoral extravasation through the EPR effect. Several possible mechanisms for interaction of liposomes with cells, after accumulation in the target tissue have been described. First of all, unspecific binding or absorption of liposomes to cells can occur, and untargeted liposomes can deliver their drug load by this mechanism. When in close contact with the cell, lipophilic drugs encapsulated in the liposomal membrane can be transferred to the cell membrane, while encapsulated hydrophilic drugs in some circumstances can be released from absorbed liposomes and taken up into the cells. Both these processes are not fully understood, but it is clear that the lipid composition of the liposomal membrane and the physiochemical characteristics of the drug in question are of great importance. Another suggested mechanism by which liposomes can deliver their content to the cellular compartment are through fusion of the liposomal lipid membrane with the cellular membrane, thereby inducing cytoplasmic release of the liposome content. However, no evidence indicate that cellular fusion occur when using standard conventional or PEGylated liposome and in general specific fusion-inducing agents are believed to be required for stimulation of this process. (16)

Two primary mechanisms have been proposed for how targeted liposomes can increase the cellular uptake of liposomes, depending on both the properties of the target molecule and the targeting ligand. When targeting the liposomes to a cell surface receptor at a site where binding induce internalization of the whole complex, the liposomes can be internalized through receptor-mediated endocytosis into the cellular compartment of the cancer cells. Like described for receptor-mediated endocytosis of liposomes by macrophages, the liposomes can now degraded by lysosomal enzymes and the drug released into the cytoplasm. However, even liposomes targeted to a non-internalizing molecule have demonstrated a higher intracellular accumulation of the transported drug. A likely mechanism is probably that binding of the liposome to its target keep the liposomes in close contact with target cells, facilitating diffusion of the encapsulated drug into the cells degradation of the bound liposome. (13, 118)

2.3.3 Liposomes in Cancer Therapy

Pathological conditions inducing an inflammatory state of the vasculature, such as infections, ischemic heart disease, and cancer, the vasculature may become leaky, permitting the liposomes to extravasate at the lesion site (16). In tumors, this is known as the EPR effect and can be exploited to passively target liposomes to the tumor tissue (57). However, to achieve significant liposomal accumulation in the tumor, the liposomes must circulate repeatedly through the tumor vessels to increase the change of extravasation. Furthermore, the pore size found in the leaky parts of the tumor vasculature vary widely according to the type and location of tumor (119). Therefore the liposome size must be carefully chosen from the experimental model used for studying the therapeutic efficacy of the liposomes. Both untargeted and targeted liposomes accumulate in tumor tissue through the EPR effect to a similar extent. The superior anticancer effects observed when using targeted liposomes loaded with chemotherapeutic drugs do therefore not stem from a higher intratumoral accumulation of the liposomes, but rather from differences in the intratumoral localization at the cellular level. After intratumoral accumulation, untargeted liposomes have been observed to reside predominantly in the interstitium, whereas targeted liposomes and especially liposomes targeted to an internalizing receptor are found intracellularly in a much higher degree. (13)

The potential of liposomes for delivering anticancer drugs have been investigated extensively in different cancer types. Especially the chemotherapeutic drug doxorubicin has received much attention,

since it is easy to load high amounts of this drug into liposomes (53). In fact, commercially available untargeted liposomes loaded with doxorubicin, marketed under the name Caelyx®, have already been approved for clinical use in several cancers (12) and have also been investigated in clinical trials for glioblastoma multiforme (56, 120). Untargeted liposomal formulations of doxorubicin benefits especially from the improved toxicity profile, but have also demonstrate some improvements in therapeutic efficacy compared to the free drug (121). So far, targeted liposomes have only been investigated in animal models of human cancers, where targeting of liposomal drugs to the cancers cells or the tumor vasculature have demonstrated a more pronounced inhibition of tumor growth than administration free drug or untargeted liposomes (13). Some recent publications employ a combination of several liposome types or conjugate a number of different targeting molecules to the surface of a single liposome, in order to achieve a more efficient tumor targeting than with only one targeting agent. Several of these studies indeed demonstrated a synergistic r effect compared to only using one targeting agent (14, 15).

2.4 Liposomal Targeting of Cancer Cells and Tumor Endothelial Cells in Glioblastoma Multiforme

A combination of liposomes targeting the cancer cells and the tumor endothelial cells of glioblastoma multiforme could possibly achieve a higher degree of tumor targeting and synergistic anticancer effects of loaded drug. Therefore the scope of this thesis was to investigate this subject in an in vitro and in vivo model of glioblastoma multiforme. To accomplish specific targeting and sufficient accumulation of the liposomes in vivo, an appropriate liposomal system had to be chosen together with specific and highly expressed molecules for targeting.

2.4.1 Target Molecules

A variety of molecules have been proposed for targeting of glioblastoma cells and the associated vasculature. However, for liposomal targeting the target molecule must be found on the cell surface and a higher cellular uptake can be achieved if the target molecule is internalized after binding of the liposome, since this has been shown to increase the cellular accumulation and therapeutic efficacy of liposomal drugs. Based on these criteria, the EGFR was chosen as the cancer cell target molecule and the VCAM-1 was chosen as the target molecule of the tumor vasculature.

The EGFR is a tyrosine kinase cell surface receptor, which induce cellular proliferation, survival and motility after activation by binding of EGF, transforming growth factor-β and its other ligands (122). As mentioned earlier, the EGFR signaling pathway is involved in the pathogenesis of especially primary glioblastoma multiforme and the therapeutic effects of molecular targeted drugs has been investigated in glioblastoma multiforme patients. Approximately 40 % of all glioblastoma cases are characterized by amplification of EGFR, and in 30 % of glioblastomas this is accompanied by the presence of a constitutively activated EGFR mutant known as EGFRvIII (123). In this mutant form of EGFR exon 2 to 7 of the EGFR have been deleted, which is a part of the extracellular domain of the receptor. This deletion results in an EGFR variant that is unable to bind ligand, but signals constitutively. (124) Cetuximab (Erbitux®) is a recombinant, human/mouse chimeric monoclonal antibody that binds to the extracellular part of both the normal human EGFR and the mutated EGFRvIII. This antibody has been approved for clinical use in therapy of metastatic colorectal cancer and head and neck squamos cell carcinoma (125), and it is currently being investigated in clinical trials for therapy of several other cancer types, including glioblastoma multiforme (126). Upon binding to the EGFR, cetuximab has been demonstrated to induce internalization of the receptor-antibody complex (127). Cetuximab or fab' fragments hereof have been used for liposomal conjugation and the resultant immunoliposomes have

demonstrated in vitro binding, internalization and cytotoxicity to cancer cells expressing EGFR or EGFRvIII (128, 129, 129-132), as well as in vivo accumulation in tumor xenografts and superior therapeutic efficacy when loaded with various chemotherapeutics compared to nontargeted liposomal or free drug (59, 132).

VCAM-1 is a cell adhesion molecule involved in transendothelial migration of leucocytes into inflamed tissues by the process known as diapedesis and mediates firm adhesion of the migrating leucocytes to the endothelium (133). Ligand binding results in internalization of VCAM-1 in endothelial cells (134). Expression of VCAM-1 is virtually absent on human vasculature of healthy tissues (135), but inflammatory cytokines such as TNF-α and IL-1 may upregulate VCAM-1 endothelial expression in pathological conditions as cancer (136, 137). In human cancers, tumor endothelial cell expression of cell adhesion molecule expression varies between specific tumor types and locally within the tumor lesion (135, 138). The altered cell adhesion molecule expression may provide a possible mechanism for tumor evasion of the immune systems, since the ordered molecular process of transendothelial leukocyte migration is disrupted (133). VCAM-1 have been used for successful endothelial cell targeting in vitro and in vivo in human cancer models, promoting cellular uptake of liposomes and targeting of the tumor endothelium (79, 139). However, so far only one published study has investigated the expression of VCAM-1 in human glioblastoma vasculature, and here VCAM-1 was expressed in the tumor blood vessels in 25 % of glioblastoma cases (140).

2.4.2 Liposomal System for Cancer Targeting

The liposome behavior in vitro and in vivo depends on the overall structure and the characteristics of its single components. A long circulation time in vivo is essential for intratumoral accumulation of liposomes via the EPR effect, and therefore small PEGylated liposomes conjugated with a moderate amount of antibody remains the preferred choice for cancer targeting applications.

Small unilammellar liposomes of a defined size can be prepared by a variety of different techniques. A simple technique widely used for preparation of such liposomes is the lipid film-hydration technique, followed by extrusion of the liposomes until researching to the desired size. A dry lipid film of the lipids desired for liposome preparation is prepared by measuring out lipids dissolved in an organic solvent such as chloroform and evaporating the solvent, dispersing a thin lipid film on the inside of the flask. Addition of an excess aqueous solution followed by mechanical agitation, result in spontaneously formation of a suspension of unhomogenous large multilammellar liposomes within the 0.5 to 10 μm range. In order to prepare a more homogeneous suspension of small unilammellar liposomes, the multilamellar liposomes can be sequentially extruded through polycarbonate membranes with decreasing pore size until the liposomes have the desired size. During extrusion the large multilammellar liposomes are forced through the pores of the polycarbonate membrane by application of pressure, resulting in transient rupture of the lipid membrane and resealing at a size closer to the pore size of the membrane. Typically, passing a suspension of large multilammellar liposomes 10 times through a membrane with a pore size of 100 nm produces a homogeneous liposome suspension with a mean diameter of approximately 100 nm. (17)

In order to direct the liposomes to either the cancer cells or the tumor endothelial cells, the chosen targeting antibodies must be conjugated to the liposomes. Coupling of the antibodies to the distal ends of the surface grafted PEG-chains have demonstrated to be superior in retaining antigen binding ability. PEG-lipids with various reactive groups at their distal end have been developed for the purpose of chemical conjugation with targeting ligands. One highly efficient and widely used method for protein conjugation involves the formation of a thioether bond between a maleimide group on the end of

the PEG-chains to a protein thiol group (141). To use this conjugation method, a free thiol group must be available in the protein for chemical reaction. Free thiol groups can be generated either by breaking endogenous disulfide bridges in the protein, if this can be done without destroying the desired properties of the targeting molecule, e.g. its binding properties, or exogenous thiols can be introduced into the protein by the use of one out of several available thiolating agents (142). One of the most advantageous thiolating agents is succinimidyl-S-acetyl thioacetate (SATA). Reacting proteins with SATA, randomly introduces thioester groups into the proteins and free thiol groups for reaction with the PEG-coupled maleimide can easily be generated by deacetylation of the thioester using hydroxylamine. The free thiol can now react with maleimide to generate a thioether bond between the liposome and the conjugated protein. The thioether bond between maleimide and thiol group of the protein is very stable in a biological environment, and this method is therefore suitable, when conjugation for a prolonged period of time is desirable (141).

Traditionally, functionalized PEG-lipids have been incorporated into liposomes by including it in the initial lipid mixture used for liposome preparation, followed by conjugated of preformed liposomes. However, drawbacks of this method include the random orientation of the functionalized PEG-molecules and PEG-chains localized in the inner leaflet of the lipid bilayer will not be accessible for ligand conjugation. To circumvent this problem, a method for post-insertion of PEG-lipids already conjugated with ligand, known as the post insertion technique (18). Here, micelles consisting of the functional PEG-lipids are initially formed and the targeting ligand conjugated to the micelles. Afterwards the micelles can be inserted into preformed liposomes, by incubating above the fase transition temperature of the lipids. Liposomes prepared by the post insertion technique have been demonstrated to have ligand densities and in vivo performance characteristics similar to liposomes prepared by the traditional approach (143). An overview of the different steps in preparation of immunoliposomes by the micelle post insertion technique can be seen in Figure 2.

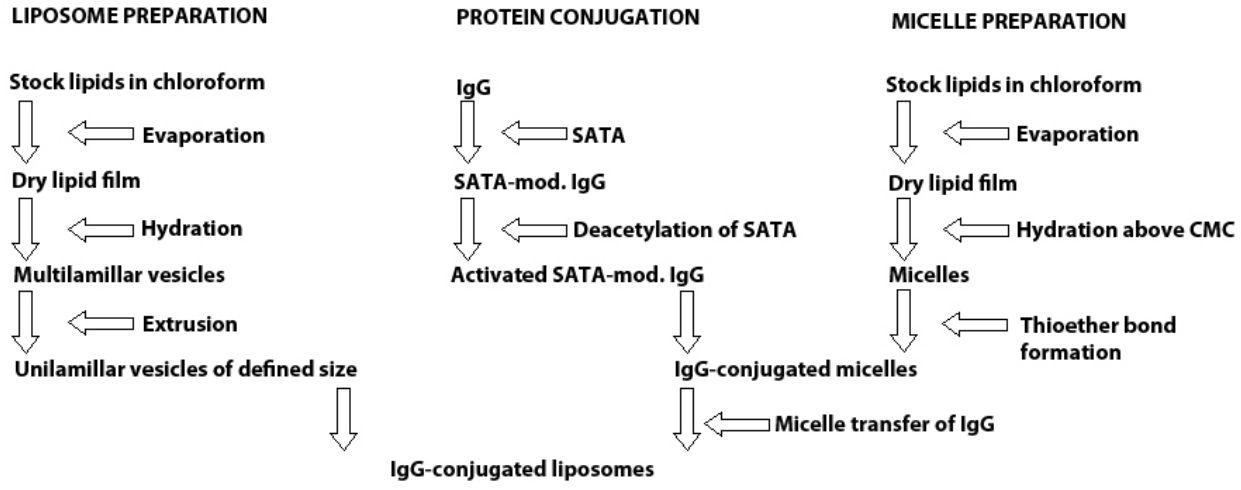

Figure 2: Overview of immunoliposome preparation by the micelle post insertion technique. This technique consists of three separate processes; preparation of liposomes by lipid-film hydration and extrusion to the desired size, modification of IgG with SATA, and preparation of micelles containing a maleimide-functionalized lipid. The micelles are then conjugated with SATA-modified IgG and insertion into the preformed liposomes.

2.4.3 In Vitro and In Vivo Model of Glioblastoma Multiforme

Cellular and animal models of human diseases constitute the first line of investigations for providing evidence of therapeutic efficacy during drug development and for studying the underlying pathophysiological mechanisms of the disease (144). In vitro models for different human cancers consist of primary cells or tissue explants obtained directly from surgical patient material or immortalized human cell lines. Since available patient material often is limited and viable cells derived hereof cannot be cultured extensively, the use of immortalized cancer cells lines is frequently preferred. Immortalized cell lines retain several essential features of the original cancer cells during serial passaging, and this trait together with their easy access and ability to be cultured indefinitely in vitro have resulted in widespread use of immortalized cancer cells lines for research purposes. However, both phenotypic and genotypic characteristics of the parent tumor can be lost during serial passaging of cells, as in vitro culture leads to cellular adaption and selection, generating a more homogenous cancer cell population than originally found in the tumor (145). One of the most widely used immortalized glioblastoma multiforme cell lines is the U-87 MG (144). This cell line was originally derived from the tumor of a 44 years old female glioblastoma multiforme patient back in the 1960es by Pontén and colleguages (146) and is still used extensively for glioblastoma research today. Retained characteristics of the original tumor by cultured U-87 MG cells include cellular and nuclear pleomorphism, expression of the astrocytic markers vimentin and fibronectin, overexpression of the EGFR, and in vivo tumorigenicity. (145)

Animal models of glioblastoma multiforme and other cancers are essential in generating sufficient therapeutic evidence for novel drugs to progress into clinical trials. The most extensively used models are various tumor xenograft models, where tumor development occurs after implantation of primary or immortalized human glioblastoma cells into an immunocompromised animal. Other glioblastoma models include transgenic or spontaneous animal models, but these models overall suffer of a high expenses and low rates of tumor development. (144) The use of U-87 MG cells for establishing tumor xenografts in rodents is well-characterized (147, 148). This can be achieved either by injecting viable U-87 MG cells subcutaneously into the flank of the animal, generating of a heterotopic tumor, or into a defined location within the brain to establish an orthotopic tumor. Establishing subcutaneous tumor xenografts involve less complicated surgical procedures compared to the orthotopic model, and tumor development can be accessed directly, as the growing tumors can be observed as lumps under the skin. In contrast, tumor growth of intracranial tumors can only be confirmed by the use of advanced imaging equipment or post-mortem. However, the resulting tumor xenografts more closely resemble naturally occurring tumors, when grown in the natural intracranial environment of glioblastoma multiforme. (144) One example includes higher degree of leakines of the vasculature in subcutaneously grown U-87 MG tumors and other xenografts compared to the orthotopic tumors, whose vessel permeability is reduced by the presence of the blood-brain barrier (119, 149). Thus, research involving blood-borne drugs that do not freely pass the blood-brain barrier should be carried out in intracranial tumor xenograft models to mirror the clinical setting more closely (144). Although immortalized cells are known to lose some of their original characteristics during in vitro culture, they still display many features of the specific cancer type when implanted in vivo. After intracranial implantation of U-87 MG cells, macroscopically visible tumors typically develop within a couple of weeks, displaying key features of glioblastoma multiforme, such as cellular pleomorphism, invasive growth, neovascularization through widespread angiogenesis, and tumor infiltration by T lymphocytes and macrophages (147). Thus, the U-87 MG cell line constitutes a well-characterized model of glioblastoma multiforme and displays glioblastoma characteristics important for investigating liposomal targeting of this cancer type.

3 MATERIALS AND METHODS

3.1

3.2 Materials

Standard chemicals were obtained from Sigma-Aldrich (Germany) or Merck (Germany) unless otherwise stated. All used reagents were of analytical grade.

3.3 Cell Culture

The human glioblastoma cell line, U-87 MG (ATCC-LCG, Sweden) was grown in Dulbecco's modified Eagle's medium (DMEM) (Sigma-Aldrich) supplemented with 10 % fetal calf serum (FCS) (Gibco, Invitrogen, UK), 100 units/ml penicillin (Gibco), and 100 µg/ml streptomycin (Gibco). The murine brain endothelial cell line, bEnd.3 (obtained from the Panum Institute, University of Copenhagen, Denmark) was grown in DMEM medium supplemented with 10 % FCS, 4 mM L-glutamine (Gibco), 100 units/ml penicillin, and 100 µg/ml streptomycin. Both cell lines were maintained at 37 °C, 5 % CO_2, and 95 % air in a humidified incubator and routinely passaged at confluency. All experiments were performed on cells seeded out 24-48 hours in advance, allowing the cells to attach to the surface of the tissue culture plate and to reach a cell density appropriate for the particular experiment.

3.4 Characterization of Target Expression by Cell Lines

The cellular expression of the cell surface molecules chosen for liposomal targeting was investigated using immunocytochemistry. The expression of EGFR by U-87 MG cells and VCAM-1 by TNF-α stimulated bEnd.3 cells were determined using the antibodies intended for liposomal conjugation as primary antibodies.

3.4.1 Immunocytochemical Detection of EGFR on U-87 MG Cells

U-87 MG cells were seeded out in 8 well LabTek permanox chamber slides (Nunc, VWR, Denmark) and grown to 60-70 % confluency. The growth medium was removed and the cells washed with potassium phosphate buffered saline (KPBS), followed by fixation in 4 % paraformaldehyde in KPBS for 5-10 minutes and washing with KPBS to remove excess fixative. The monoclonal chimeric human/mouse-anti-human EGFR antibody Erbitux® (Merck, obtained from Nomeco A/S, Aalborg, Denmark) was added to each well at various concentrations ranging from 5 to 100 µg/ml in incubation buffer (3 % goat serum (Biological Industries, In Vitro, Denmark), 2 % bovine serum albumin (BSA) (Sigma-Aldrich), and 0.3 % Triton X-100 in KPBS) and incubated at 4 °C overnight. The goat serum and BSA included in the incubation buffer block unspecific binding of antibody, whereas Triton X-100 permeabilizes the cell membrane. The next day, the cells were washed with washing buffer (incubation buffer diluted 1:50 in KPBS) to remove excess primary antibody. Secondary antibody Alexa Fluor 488 goat-anti-human IgG (H + L) (Molecular Probes, Invitrogen, UK) diluted 1:200 in KPBS was added to each well and incubated for 30 minutes at room temperature to visualize bound primary antibody. The cells were then washed in KPBS to remove excess secondary antibody. To allow identification of cell nuclei, the cells were stained for 10 minutes with 50 µg/ml 4',6-diamidino-2-phenylindole (DAPI) (Sigma-Aldrich) in KPBS and excess stain was removed by washing with KPBS. Afterwards, the well chambers and gaskets were carefully removed and coverslips were mounted with fluorescence mounting medium (Dako, Denmark). Negative controls were obtained by following the same procedure, except for omission of the primary antibody. The cells were visualized under a non-inverted fluorescence microscope

(Axioplan 2 imaging, Carl Zeiss, Germany) and images were obtained with camera (AxioCam MRc, Carl Zeiss).

3.4.2 Immunocytochemical Detection of VCAM-1 on bEnd.3 cells

bEnd.3 cells were seeded out in 8 well LabTek permanox chamber slides and grown to 60-70 % confluency. To determine a suitable setup to enhance expression of VCAM-1, the bEnd.3 cells were activated with various concentrations of recombinant murine TNF-α (Sigma-Aldrich) ranging from 0 to 100 ng/ml and at various time periods ranging from 1 to 24 hours. The growth medium was then removed and the bEnd.3 cells were fixed in 4 % paraformaldehyde in KPBS, immunostained for VCAM-1, DAPI stained, and mounted with coverslips according to section 3.4.1. VCAM-1 was detected using monoclonal rat-anti-mouse VCAM-1 antibody (clone M/K-2, Abcam, UK) diluted 1:100 in incubation buffer and secondary antibody Alexa Fluor 488 goat-anti-rat IgG (H + L) (Molecular Probes) diluted 1:200 in KPBS. The cells were visualized under a non-inverted fluorescence microscope and images were obtained with camera.

3.5 Animals

Male CD1 nude mice were purchased from Taconic (Silkeborg, Denmark), and housed in a temperature- and humidity-controlled ventilated filter cabinet (Scantainer, Scabur, Denmark) to protect the animals from contamination and infection. The cabinet were kept in a room with a 12 h light/12 h dark schedule. The animals were allowed free access to food and water. Daily care was performed by the staff at the animal facility at Sygehus Nord, Aalborg, where all the animal experiments were carried out. The experiments were initiated when the nude mice were 6 to 10 months old. All surgical procedures were approved by Rådet for Dyreforsøg, Dyreforsøgstilsynet, under the Danish Ministry of Justice.

3.6 Intracranial Tumor Xenograft Model

An intracranial model of U-87 MG glioblastoma was established in CD1 nude mice and the tumors was characterized with respect to their growth pattern, vascular permeability, and expression of cell surface molecules for liposomal targeting. The xenograft model was in addition used for studying the in vivo biodistribution of unconjugated liposomes.

3.6.1 Intracranial Model of U-87 MG Glioblastoma in Nude Mice

For establishment of intracranial tumor xenografts, U-87 MG glioblastoma cells were harvested by trypsinization, washed two times in sterile PBS, and resuspended in sterile PBS at a concentration of 5 x 10^5 or 1 x 10^6 U-87 MG cells per 5 µl. The nude mice (n = 3) were anesthetized by intraperitoneal injection of 0.5-0.75 ml/100 g body weight of Hypnorm (fetanyl citrate 0.315 mg/ml, fluanisone 10 mg/ml, VetaPharma, UK), Dormicum (midazolam 5 mg/ml, Roche, Germany) and sterile water in a ratio of 1:1:2. The animals were placed in a small animal stereotactic apparatus (Stoelting Lab Standard with mouse & neonatal rat adaptor, Stoelting, Ireland). The dorsal head surface was disinfected with a 1 % hydrogen peroxide solution, and the skin incised at the midline and retracted. The exposed area of the scalp was blotted dry. A small burr hole was made 1.1 mm dorsal to and 1.5 mm right to the bregma. Each mouse received a stereotactically guided injection of 5 x 10^5 (n = 2) or 1 x 10^6 U-87 MG cells (n = 1) in 5 µl of sterile PBS in the right striatum (1.1 mm lateral and 1.1 mm dorsal to the bregma, at 3.5 mm depth from the skull surface) using a Hamilton syringe. The U-87 MG cells were injected slowly to avoid elevation of the intracranial pressure, and the syringe was left for five minutes to pre-

vent inoculated cells from ascending through the track of the needle. The skin edges were sutured, and the animals were returned to their cages and placed under a heat lamp. The animals were monitored during recovery from anesthesia, and then daily. The mice were terminated at signs of considerable tumor burden, defined as loss of more than 20 % of baseline body weight, and neurological signs of increased intracranial pressure, e.g. gait or balance difficulties.

3.6.2 Animal Euthanasia

The nude mice were anesthetized by intraperitoneal injection of 0.5-0.75 ml/100 g body weight of Hypnorm, Dormicum, and sterile water in a ratio of 1:1:2 and subsequently sacrificed by transcardial perfusion fixation. One mouse was injected intraperitoneally with 0.5 % peroxidase (Sigma-Aldrich) in sterile PBS approximately 1 hour before euthanasia to study vascular permeability in the tumor. For euthanasia, an incision was made through the abdomen just below the rib cage, together with two horizontal cuts through the rib cage on either side of the heart, followed by exposure of the heart by flipping the cut rib flap upwards to the head. An escape route for blood and perfusion fluid was made by cutting an opening in the right atrium. A small incision was made at the apex of the left ventricle, the needle of a syringe filled with KPBS inserted and perfusion initiated. When the fluid appeared clear, the syringe was removed, and a syringe containing 4 % paraformaldehyde in KPBS was inserted instead and the animals were perfused with fixative. The brains were removed from the skull, immersed in 4 % paraformaldehyde in KPBS at 4 °C for 24 hours for post-fixation, followed by short-time storage in KPBS at 4 °C until further processed for histological analysis.

3.7 Characterization of Intracranial Tumor Xenografts

The growth pattern of the tumor xenografts was characterized using cresyl violet staining of cell bodies and glial fibrillary acidic protein (GFAP) immunostaining of astrocytes to localize cancer cells in brain cryostat sections. The vascular permeability of the tumor vessels were studied by visualizing the intratumoral distribution of mouse albumin by immunostaining, and by staining brain sections from the peroxidase-perfused animal with 3,3'-diaminobenzidine (DAB). Furthermore, the expression of EGFR and VCAM-1 within the tumor area was investigated by immunostaining using the antibodies intended for liposomal conjugation as primary antibodies.

3.7.1 Cryostat Sectioning of Mouse Brains

Prior to sectioning the mouse brains were infiltrated with 20 % sucrose for 2-3 days to cryopreserve the tissue during cryostat sectioning. The brains were embedded in Tissue-Tek (Sakura, Finetek Europe B.V., Netherlands) and sectioned in 40 µm thick serial, coronal slices using a cryostat (Microtome cryostat, HM 505 N, Microm, Germany). Tissue-Tek was dissolved by immersing the sections in KPBS, and afterwards the sections were stored in antifreeze (30 % sucrose, 30 % ethylene glycol, and 10 % polyvinylpyrrolidone in PBS) at -20 °C until staining.

3.7.2 Cresyl Violet Staining

Mouse brain sections were washed in KPBS, mounted onto slides and air-dried at 37 °C until completely dry. The sections were then defatted overnight in a solution of ethanol and chloroform in a volume ratio of 1:1. The next day, the sections were rehydrated with decreasing concentrations of ethanol to distilled water. Cresyl violet solution (0.4 % cresyl violet (Sigma-Aldrich), 1 M sodium acetate, 1 M acetic acid) preheated to 37 °C was added to each section and incubated for 5 minutes at room temperature. Excess stain was removed by rinsing the sections in water. The sections were then differen-

tiated for 10-15 minutes in 96 % ethanol, dehydrated in 99.9 % ethanol, and cleared in xylene. Coverslips were mounted with pertex mounting media (Leica Microsystems, Denmark). Stained brain tissue was visualized under a non-inverted microscope and images were obtained with camera.

3.7.3 Immunohistochemical Detection of GFAP and Mouse Albumin

Mouse brain sections were washed in KPBS and free floating sections were stained according to the principle described for immunocytochemistry in section 3.4.1. The primary antibody solutions were polyclonal rabbit-anti-GFAP (Dako) at a 1:200 dilution in incubation buffer (3 % pig serum (Sigma-Aldrich) and 0.3 % Triton X-100 in KPBS), or polyclonal rabbit-anti-mouse albumin (Nordic Immunology, Nordic BioSite Aps, Denmark) at a 1:1000 dilution in incubation buffer. For both primary antibodies, the secondary antibody solution was Alexa Fluor 488 goat-anti-rabbit IgG (H + L) (Molecular Probes) diluted 1:200 in KPBS. After immunostaining, the sections were arranged on slides and mounted with fluorescence mounting medium. Negative controls were obtained by following the same procedure, except for omission of the primary antibody. Immunostained brain tissue was visualized under a non-inverted fluorescence microscope and images were obtained with camera.

3.7.4 DAB Staining of Peroxidase-Perfused Brain Tissue

Brain sections from the mouse perfused with peroxidase prior to euthanasia were reacted with the peroxidase substrate DAB to study accumulation of peroxidase in the tumor xenograft. Free floating unstained sections or sections immunostained for GFAP according to section 3.7.3 were washed in KPBS and afterwards in Tris-HCl (pH 7.6). DAB solution (0.05 % DAB (Sigma-Aldrich) and 0.01 % H_2O_2 Tris-HCl (pH 7.6)) were added to the sections and incubated for 10 minutes at room temperature to reveal tissue peroxidase activity. Sections were then washed in KPBS to remove excess DAB substrate. The sections were arranged on slides and mounted with pertex mounting medium. Brain sections from the mouse not perfused with peroxidase prior to euthanasia were staining following the same procedure and used as negative controls. Immunostained brain tissue was visualized under a non-inverted fluorescence microscope and images were obtained with camera.

3.7.5 Immunohistochemical Detection of EGFR and VCAM-1

Mouse brain sections were washed in KPBS and free floating sections were stained according to the principle described for immunocytochemistry in section 3.4.1. The primary antibody solutions were monoclonal chimeric human/mouse-anti-human EGFR antibody Erbitux® at a 1:100 dilution in incubation buffer (3 % goat serum, 2 % bovine serum albumin (BSA) and 0.3 % Triton X-100 in KPBS), or monoclonal rat-anti-mouse VCAM-1 antibody at a 1:100 dilution in incubation buffer. Alexa Fluor 488 goat-anti-human IgG (H + L) secondary antibody diluted 1:200 in KPBS was used for detection of EGFR and Alexa Fluor 488 goat-anti-rat IgG (H + L) secondary antibody diluted 1:200 in KPBS for detection of VCAM-1. After immunostaining, the sections were arranged on slides and mounted with fluorescence mounting medium. Negative controls were obtained by following the same procedure, except for omission of the primary antibody. The cells were visualized under a non-inverted fluorescence microscope and images were obtained with camera.

3.8 Preparation and Characterization of Immunoliposomes

Erbitux®-liposomes, anti-VCAM-1-liposomes, and unconjugated control liposomes were prepared by insertion of micelle-conjugated antibodies into preformed liposomes. DSPE-PEG2000-maleimide was used as the micellar anchor for attachment of SATA-modified antibodies. The final liposome suspen-

sions were characterized with respect to particle size, zeta potential, lipid concentration, and conjugated antibody.

3.8.1 Preparation of Liposomes

Liposomes were prepared from soy phosphatidyl choline, cholesterol, 1,2-dipalmitoyl-sn-glycero-3-phosphoethanolamine-N-[methoxy-(polyethylene glycol)-2000] (mPEG2000-PE), and 3,3'-dioctadecyloxacarbocyanine perchlorate (DiO) in a molar ratio of 65:33:2:0.5. All lipids were obtained from Avanti Polar Lipids (Alabaster, Alabama, USA) and the fluorescent probe DiO from Sigma-Aldrich. Lipids dissolved in chloroform were transferred to a round-bottom flask, and a thin lipid film was prepared by whirling the flask during evaporation of chloroform with a stream of nitrogen. Afterwards the flask was kept under a stream of nitrogen for 30 minutes, to ensure evaporation of residual chloroform. The lipid film was hydrated in HEPES buffer (10 mM HEPES (pH 7.5), 136 mM NaCl, 1 mM EDTA) at a final lipid concentration of 30 mM on a shaker for one hour and occasionally vortexed vigorously, forming multilamellar liposomes of heterogeneous size. The extrusion technique was then used to form unilammellar liposomes with a size averaging 100 nm. The liposome dispersion was repeatedly passed through polycarbonate membranes (Nucleopore Track-Etch Membrane Filtration Products, Whatman, Avanti Polar Lipids) with 0.2 μm and subsequently 0.1 μm pore size, using a hand held Mini-Extruder (Avanti Polar Lipids).

3.8.2 Preparation of Micelles

Micelles were prepared from 1,2-distearoyl-sn-glycero-3-phosphoethanolamine-N-[maleimide (polyethylene glycol)-2000] (DSPE-PEG2000-maleimide)(Avanti Polar Lipids) and mPEG2000-PE in a molar ratio of 4:1. Lipids dissolved in chloroform were transferred to a round-bottom flask, the chloroform was evaporated with a stream of nitrogen, and the flask was left under a stream of nitrogen for 30 minutes. The lipids were hydrated in HEPES buffer preheated to 65 °C, at a final lipid concentration of 10 mM, which is above the CMC of the two lipids. Micelles were formed by heating the lipids to 65 °C in a heating block (Thermomixer comfort, Eppendorf, Eppendorf Nordic Aps, AH Diagnostics) during vigorous agitation for 1 hour.

3.8.3 Antibody Conjugation to Micelles

The monoclonal chimeric human/mouse-anti-human EGFR antibody Erbitux® was used for preparation of anti-EGFR-liposomes and the monoclonal rat-anti-mouse VCAM-1 antibody for preparation of anti-VCAM-1-liposomes, while control liposomes were left unconjugated. If the antibody buffer solution contained stabilizing proteins, free amino acids, or other molecules containing free amino groups, the buffer was exchanged prior to conjugation, to prevent the free amino groups of these molecules to compete with the antibodies for reaction with SATA. PD-10 desalting columns (GE Healthcare, UK) were used for exchanging the antibody buffers to HEPES buffer by gel filtration chromatography according to manufacturer's instructions for the spin protocol. The protein concentration of the eluate was determined by UV spectroscopy (NanoPhotometer, Implen, Germany), measuring the absorbance at 280 nm. SATA modification of the antibodies was carried out by mixing SATA (Pierce, VWR, Denmark) dissolved in N-N-dimethylformamide with the antibody solution in a volume ratio of 1:100 for N-N-dimethylformamide:IgG solution and a molar ratio of 8:1 for SATA:IgG. The mixture was incubated for 45 minutes at room temperature during continuous rotation. Using a Vivaspin 6 ultrafiltration device (GE Healthcare) with a 50,000 kDa molecular weight cut off membrane, free SATA was removed and the antibodies concentrated to approximately 1 ml in volume by centrifugation accord-

ing to manufacturer's instructions. The protein concentration was determined using UV spectroscopy as described above, and the modified antibodies were stored at -20 °C until use. Before conjugation of antibodies to micelles the SATA groups must be deacetylated, creating free sulfhydryl groups to react with the maleimide anchor in the micelles. Deacetylation was conducted by adding a freshly prepared hydroxylamine solution (0.5 M hydroxylamine HCl, 0.5 M HEPES (pH 7.5), and 25 mM EDTA) to the antibody solution at a volume ratio of 1:10 for hydroxylamine solution:IgG solution and incubating for 1 hour at room temperature during continuous rotation. Conjugation was performed by mixing deacetylated antibodies with micelles in a molar ratio of 1:10 for IgG:DSPE-PEG2000-maleimide, incubating the solution for 2 hours at room temperature and afterwards overnight at 4 °C.

3.8.4 Micelle Transfer of Antibodies to Liposomes

IgG-conjugated micelles were mixed with preformed liposomes in a molar ratio of 0.05:1 for micelle phospholipid:liposomal soy phosphatidyl choline and incubated in a heating block (Thermomixer comfort) for 1 hour at 60 °C during continuous rotation. The liposome-micelle suspension was cooled down, and unbound antibody and micelles was separated from the immunoliposomes by gel filtration chromatography using a 4B sepharose column (Sigma-Aldrich).

3.8.5 Measuring Particle Size and Zeta Potential

Mean particle size of the various liposomes was determined by dynamic light scattering and the zeta potential by laser Doppler electrophoresis at 25 °C using a Zetasizer Nano ZS (Malvern, UK). Particle size determined by dynamic light scattering is based on the principle that the random Brownian motion of particles in a liquid is faster for small particles than for large particles. The Brownian motion of a particle is measured by illumination of the sample with a laser, and the rate of intensity fluctuation in the light scattered by a single particle is used to determine the diffusion coefficient. Using the value of this coefficient the size of the particle can be determined from the Einstein-Stokes equation. (150) Determination of particle size using the Zetasizer Nano ZS generates a Z-average value of mean particle size, polydispersity of the size distribution, and the mean size of individual peaks present in the particle suspension. The Z-average is generally considered a suitable measure of the particle size, when the width of the size distribution is narrow, generating a polydispersity value below 0.5. The zeta potential of a particle is a potential that exist between the surface of the particle and the dispersing liquid at the so-called slipping plane. The slipping plane is the boundary, where ions of opposite charge shifts from travelling with the particle through the liquid to not following the particle. The zeta potential can be measured using a combination of electrophoresis and laser Doppler velocimetry, called laser Doppler electrophoresis. When applying an electrical field to the sample, laser Doppler velocimetry can be used to measure the electrophoretic mobility, which is a measure of how fast a particle moves in the liquid. Using the value of the electrophoretic mobility the zeta potential can now be calculated from the viscosity and dielectric constant of the sample using the Henry equation. (150)

3.8.6 Determination of Phosphatidyl Choline Concentration

Phosphatidyl choline concentrations of the final liposome suspensions were determined using a phosphatidyl choline assay kit (Biovision, California, USA) in order to estimate the total lipid concentration. The assay exploits the ability of horseradish peroxidase to oxidize the colorless and nonfluorescent OxiRed probe (Amplex Red, 10-acetyl-3,7-dihydrophenoxazine) in the presence of hydrogen peroxide and generate the highly fluorescent probe, resorufin (151). The phosphatidyl choline content of each sample is indirectly quantified in the assay by enzymatic hydrolysis of phosphatidyl choline, liberating

free choline, which subsequently is oxidized by choline oxidase to betaine and hydrogen peroxide. The hydrogen peroxide generated by this reaction can now react with the OxiRed probe in 1:1 stoichiometry to generate resorufin. (152) The assay was performed according to manufacturer's instructions for the colorimetric assay. Briefly, a phosphatidyl choline standard curve consisting of 5 dilutions ranging from 1 to 5 nmol per sample was prepared. The liposomes were diluted to several concentrations to ensure that the sample readings were within the linear part of the standard curve. All standards and samples were prepared in duplicate. Reaction mix containing assay buffer, phosphatidyl choline converting enzyme, development mix, and the phosphatidyl choline probe were added to all standards and samples, and after thorough mixing the reaction was allowed to develop for 30 minutes at room temperature. Absorbance was read at 570 nm using a spectrophotometer (NanoPhotometer, Implen) equipped with a quartz ultra-micro cell (Hellma, VWR, Denmark). All readings were corrected for background by subtracting the value of the 0 phosphatidyl choline control with 0 nmol per sample. Phosphatidyl choline concentration of each sample was calculated from the plotted standard curve, and from these values the total lipid concentration was estimated, assuming that phosphatidyl choline comprises approximately 65 mol% of the final liposomes.

3.8.7 Determination of Antibody Concentration

The concentrations of conjugated antibodies were determined using the RC DC Protein Assay (Bio-Rad, Denmark). The assay is based on the Lowry assay (153), which exploits the ability of peptide bonds to react with copper under alkaline conditions, liberating Cu^{+} that subsequently reduce the Folin-phenol reagent (phosphomolybdotungstate) to heteropolymolybdenum blue. This reaction is not fully understood, but depends on copper-catalyzed oxidation of aromatic amino acids, and therefore development of the blue color is affected by the tyrosine and tryptophan content of the specific protein. (154) In contrast to the original Lowry assay, the RC DC Protein Assay is compatible with reducing agents and detergents present in the samples. Antibody concentration was measured according to manufacturer's instructions for the microfuge tube assay protocol. A standard curve consisting of 5 dilutions ranging from 0.2 mg/ml to 1.5 mg/ml human serum IgG (Sigma-Aldrich) in HEPES buffer was prepared. Liposome samples were diluted 1:5 in HEPES buffer to ensure that the sample readings were within the linear part of the standard curve. All standards and samples were prepared in duplicate. First the protein was precipitated by addition of RC reagent I and II to all standards and samples. After centrifugation the supernatant were discarded from the samples, removing any soluble interfering agents, and reagent A' was added to each sample to dissolve the precipitated protein. Reagent A containing alkaline copper tartarate solution was added to each tube and incubated with the samples to allow copper to react with the proteins. Reagent B containing a dilute Folin reagent was added to the samples, the samples was vortexed immediately, and the color reaction allowed to develop for 15 minutes at room temperature. Absorbance was read at 750 nm using a spectrophotometer (Genesys 10 UV-Vis Scanning, Thermo Fischer Scientific, Denmark) equipped with disposable semi-micro polystyrene cuvettes (Sarstadt, Germany). The antibody concentrations of the various liposome preparations were calculated from the plotted standard curve, and using the estimated total lipid concentration determined according to section 3.8.6, the amount of conjugated antibody per nmol liposome was calculated. Furthermore, the number of conjugated antibody molecules per liposome was calculated based on the assumption that a 100 nm liposome contains approximately 100,000 molecules of phospholipid (155).

3.9 In Vitro Cellular Binding and Uptake of Liposomes

The cellular uptake of liposomes by U-87 MG and bEnd.3 cells was investigated in vitro to determine the uptake of targeted liposomes compared to untargeted. After incubation of green fluorescent liposomes with cultured cells the cellular uptake of liposomes were visualized by fluorescence microscopy and quantified by flow cytometer analysis.

3.9.1 Fluorescencence Microscopy

U-87 MG and bEnd.3 cells were seeded out in separate 8 well LabTek permanox chamber slides and allowed to adhere for 24 hours. Before incubation with liposomes, the bEnd.3 cells were activated with 50 ng/ml TNF-α for 4 hours to enhance expression of VCAM-1. Immunoliposomes or unconjugated control liposomes were added to each well at a concentration of 75 nmol per 1 x 10^5 seeded cells and incubated with the cells for 2 hours at 37 °C in normal cell culture medium. Unbound liposomes were then removed by washing with PBS. The cells were fixed in 4 % paraformaldehyde in KPBS, DAPI stained, and mounted with coverslips according to section 3.4.1. The cells were visualized under a non-inverted fluorescence microscope and images were obtained with camera.

3.9.2 Flow Cytometer Analysis

U-87 MG and bEnd.3 cells were seeded out in separate well plates and allowed to adhere for 24 hours. Before incubation with liposomes, the bEnd.3 cells were activated with 50 ng/ml TNF-α for 4 hours to enhance expression of VCAM-1. Immunoliposomes or unconjugated control liposomes were added to each well at a concentration of 75 nmol per 1 x 10^5 seeded cells and incubated with the cells for 2 hours at 37 °C in normal cell culture medium. The cells were harvested by trypzination and unbound liposomes were removed by extensive washing with PBS containing 1 mM $CaCl_2$ and 0.5 mM $MgCl_2$. The cells were resuspended in PBS, and the cellular uptake of fluorescent liposomes was analyzed on a flow cytometer (FACS-Canto, BD Biosciences, Denmark) and data analyzed using FACSDiva software.

3.10 In Vivo Biodistribution of Liposomes

The accumulation of untargeted liposomes in various organs and tissues relevant to liposomal pharmacokinetics and pharmacodynamics was investigated in vivo. The aims of the experiment were to test the in vivo stability of the liposomal formulation, to develop an appropriate method for quantification of liposomal tissue accumulation, and to study the biodistribution of the untargeted liposomes.

3.10.1 Liposome Injection and Tissue Collection

Intracranial U-87 MG xenografts were established in nude CD 1 mice (n = 3) according to section 3.6.1. After development of tumors, the nude mice (n = 2) were injected i.v. with 0.5 µmol of unconjugated liposomes per mouse in sterile PBS. 24 hours later the animals were anesthetized by intraperitoneal injection of 0.5-0.75 ml/100 g body weight of Hypnorm, Dormicum, and sterile water in a ratio of 1:1:2. A blood sample was collected from each animal by heart puncture with a heparinized syringe, followed by transcardial perfusion with KPBS according to section 3.6.2. The blood samples were centrifuged for 10 minutes at 4 °C at 3000 RPM, plasma collected and stored at -80 °C until analysis. Organs and tissues of interest (brain, heart, lung, liver, kidney, spleen, muscle, and skin) were removed and cut into smaller tissue pieces. Some of each tissue was fixed in 4 % paraformaldehyde in KPBS overnight followed by short-term storage in KPBS at 4 °C until sectioning, while other tissue pieces were weighed and stored at -80 °C. Control tissue samples were obtained from an adult male Wistar

rat which had not received any liposomal injection prior to euthanasia. Blood sample, organs, and tissues were collected and stored as described above for the nude mice.

3.10.2 Fluorescence Microscopy of Tissue Sections

Fixated tissues were sectioned on a cryostat as described in section 3.7.1. Tissue sections were either mounted onto slides after washing free-floating sections in KPBS, or transferred directly to slides during sectioning. Coverslips were mounted with fluorescence mounting media, before visualizing the liposomal tissue distributions under a non-inverted fluorescence microscope and obtaining images with camera.

3.10.3 Fluorescence Spectroscopy Analysis of Tissue Homogenates

Unfixed, frozen tissue samples were homogenized completely in 800 µl of homogenization buffer (PBS or PBS with 0.5 % Tween-20) using an Ultra-Turrax T25 homogenizer (Ika, Germany). The liposomal uptake in different tissues was now quantified by fluorescence spectroscopy of tissue homogenates. A standard curve consisting of 5 dilutions of unconjugated liposomes in each of the homogenization buffers ranging from 0.15 pmol to 1.5 nmol lipid per µl was prepared. Tissue homogenate samples were diluted to several concentrations to ensure that the sample readings were within the linear part of the standard curve. All standards and samples were prepared in duplicate. Fluorescence was measured at an excitation wavelength of 457 nm and an emission wavelength of 532 nm using a fluorescence spectrophotometer (Infinite M1000, Tecan, Germany). The fluorescence intensity of each sample was normalized by the amount of homogenized tissue.

4 RESULTS

4.1 Characterization of Target Expression by Cell Lines

4.1.1 Expression of EGFR by U-87 MG Cells

Expression of the target molecule EGFR chosen for directing liposomes to glioblastoma cells was investigated by immunostaining of fixated U-87 MG cells. The chimeric anti-human EGFR-antibody Erbitux® was used as the primary antibody. This monoclonal antibody formulation is intended for clinical use in cancer therapy and no guidelines is available regarding the optimal concentration of this antibody for immunostaining. Therefore a wide range of primary antibody concentrations was tested, ranging from 5 to 100 µg/ml. Only images of EGFR immunostaining using a concentration of 50 µg/ml Erbitux® are shown (Figure 3). Staining of U-87 MG cells was observed from 5 ug/ml of primary antibody and the staining intensity enhanced with increasing primary antibody concentration until 50 ug/ml. No increase in the intensity of cellular staining was observed from 50 to 100 ug/ml of primary antibody. By comparing nuclear DAPI staining (Figure 3A) and EGFR staining (Figure 3B) of U-87 MG cells, it could be observed that the EGFR staining was primarily confined to the cell membrane, accompanied by some cytoplasmic staining. The negative control with no primary antibody added showed no cell membrane reactivity, but an unspecific, vague cytoplasmic staining (data now shown). Based on these data, a primary antibody concentration of 50 ug/ml Erbitux® was chosen for immunohistochemical staining of EGFR in U-87 MG tumor xenografts.

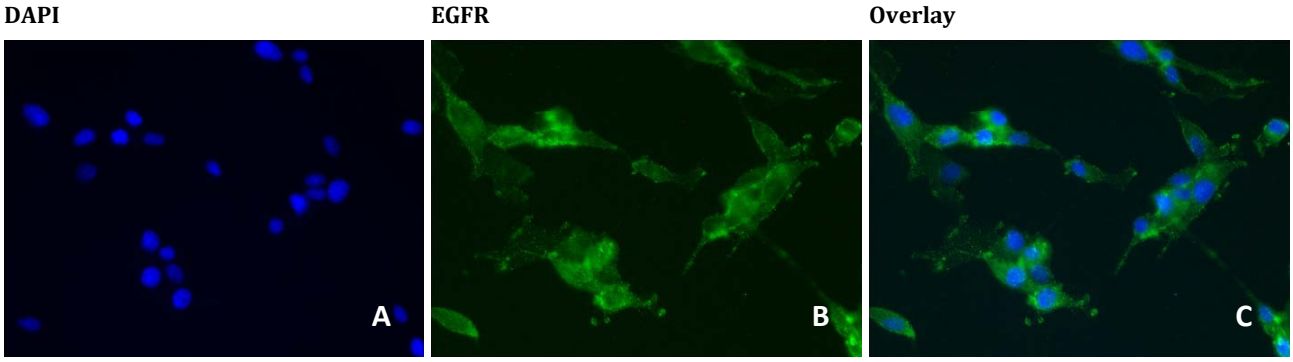

Figure 3. EGFR expression by U-87 MG cells. Immunocytochemical staining shows EGFR expression primarily confined to the cell membrane of U-87 MG cells. A) DAPI staining of cell nucleus. B) EGFR staining of cells using 50 ug/ml Erbitux® primary antibody. C) Overlay of A and B. All images: 400x magnification.

4.1.2 Expression of VCAM-1 by bEnd.3 Cells

Expression of the target molecule VCAM-1 chosen for directing liposomes to tumor endothelial cells was investigated by immunostaining of fixated bEnd.3 cells. Prior to fixation bEnd.3 cells were activated with TNF-α at various concentrations from 0 to 100 ng/ml for time periods varying between 1 and 24 hours, in order to determine a suitable setup for enhancing the cellular expression of VCAM-1. Only images of VCAM-1 immunostaining of cells incubated with 50 ng/ml TNF-α for 4 hours are shown (Figure 4). Selective staining of a few bEnd.3 cells was observed at 0 ng/ml TNF-α, and the number of reactive cells increased with higher concentrations of TNF-α up to 25 ng/ml as well as with prolonged incubation periods up to 10 hours. The maximal achieved reactivity for VCAM-1 was about 50 % of all cells. In contrast, the intensity of cellular staining was only slightly enhanced by increasing the concen-

tration or the time of TNF-α treatment. By comparing nuclear DAPI staining (Figure 4A) and VCAM-1 staining (Figure 4B) of bEnd.3 cells, it could be observed that VCAM-1 staining was primarily confined to the cell membrane. No immunoreactivity was detected in the negative control without primary antibody (data now shown). Based on the degree of VCAM-1 expression and practical issues regarding incubation time, activation of bEnd.3 cells with 50 ng/ml TNF-α for 4 hours was chosen as a suitable setup for upregulating VCAM-1 in further experiments.

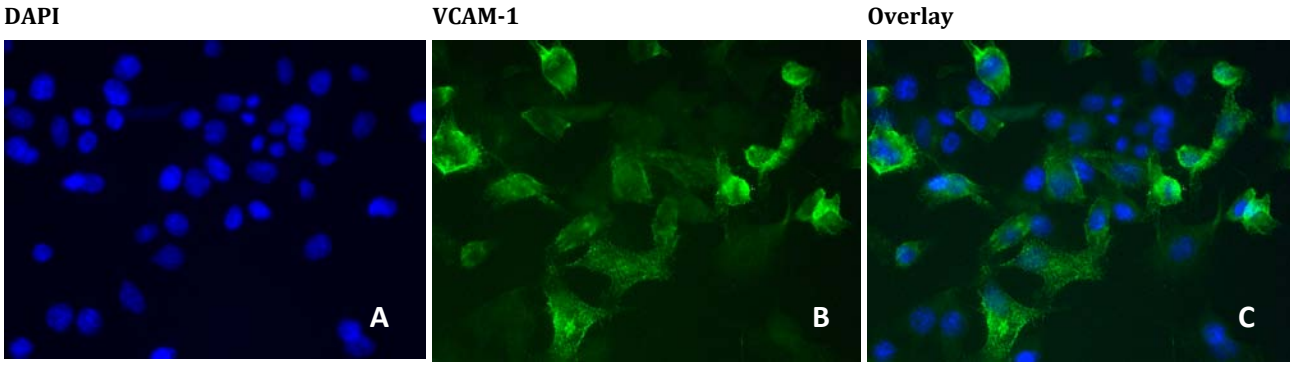

Figure 4. Expression of VCAM-1 by bEnd.3 cells. Immunocytochemical staining shows VCAM-1 expression confined to the cell membrane of bEnd.3 cells. A) DAPI staining of cell nucleus. B) VCAM-1 staining of cells treated with 50 ng/ml TNF-α for 4 hours. C) Overlay of A and B. All images: 400x magnification.

4.2 Characterization of Intracranial Tumor Xenografts

4.2.1 Cresyl Violet Staining

In order to establish an in vivo model of glioblastoma multiforme, three nude mice were stereotactically inoculated with U-87 MG cells in the striatum. Two mice were inoculated with 5 x 10^5 cells and one with 1 x 10^6 cells to assess the number of U-87 MG cells adequate for establishing an intracranial tumor xenograft. At day 17 after cell inoculation, the mouse that had received 1 x 10^6 cancer cells gradually began losing weight, indicating considerable tumor burden. At day 20, one of the mice, receiving 5 x 10^5 cancer cells, also displayed a successive weight loss, whereas the last mouse did not develop any signs of tumor formation. Brain sections from the two mice displaying consecutive weight loss were examined for tumor growth by cresyl violet staining and immunostaining for GFAP. Cresyl violet staining of cell bodies in the brain sections allowed identification of tumor growth in the brains of both mice (Figure 5). The tumor developed in the mouse inoculated with 1 x 10^6 U-87 MG cells was very large and at the maximal tumor diameter it took up most of the right subcortical brain area, making it difficult to determine the exact location of the tumor (Figure 5A). The size of the tumor developed in the brain of the mouse inoculated with 5 x 10^5 cells was much smaller compared to the tumor generated from 1 x 10^6 cells, but still it displayed a significant tumor burden, comprising more than a tenth of the total brain area at its maximal size (Figure 5B). Furthermore, this tumor had grown into the right lateral ventricle, and it appeared that some of the cancer cells had escaped from the primary tumor and spread through the ventricular system to the contralateral side of the brain. At high magnification, histological differences between the tumor and the normal brain tissue were obvious. The cells localized in the tumor tissue exhibited several classical cancer cell characteristics, including heterogeneous cell size and morphology, high cellular density, and lack of histological organization (Figure 5C). In comparison, the normal brain tissue was clearly organized in a cellular pattern, and within each cellular compartment of this pattern the cells were rather homogeneous with respect to size and morphol-

ogy (Figure 5D). Based on these histological differences, a clear-cut border could be observed at the transition from normal brain tissue to the tumor (Figure 5E).

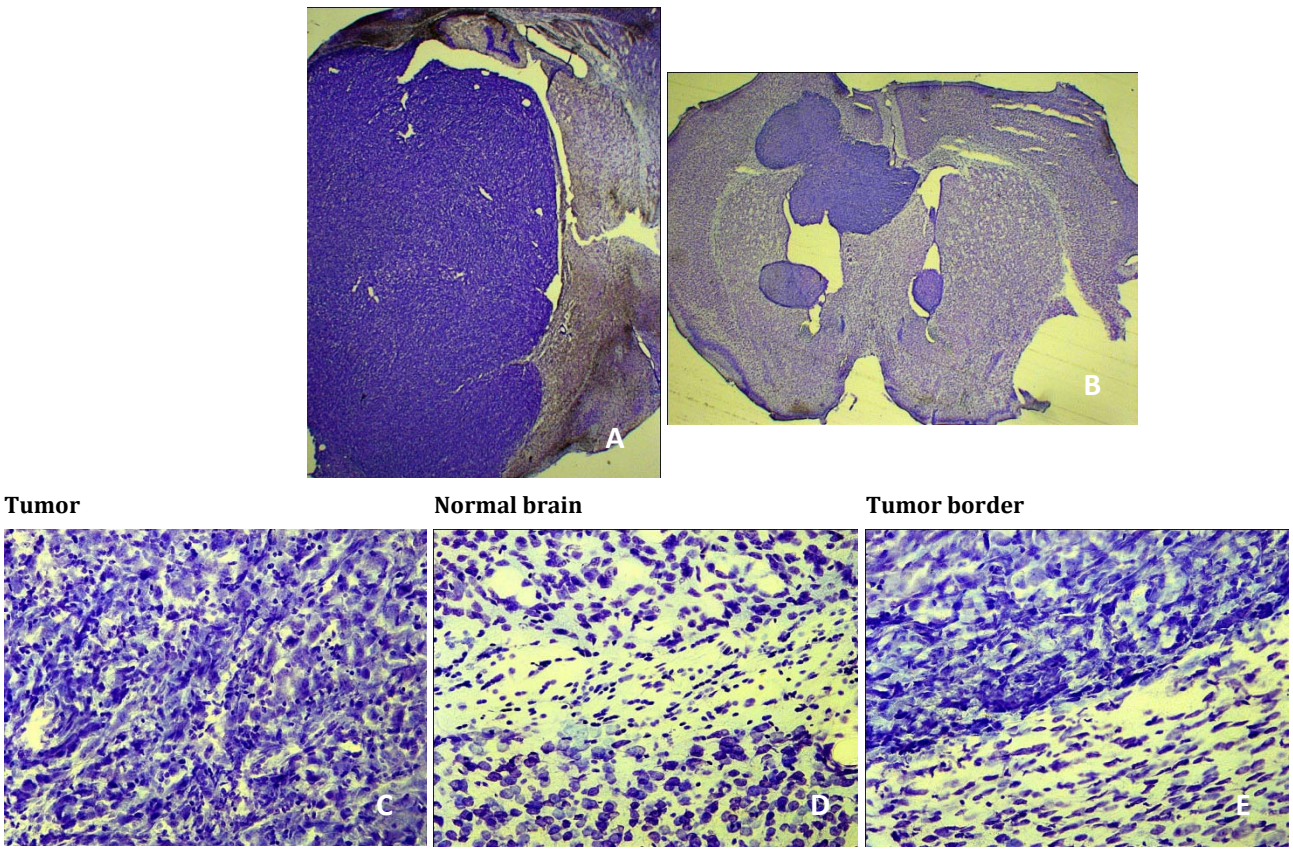

Figure 5. Cresyl violet staining of U-87 MG tumor xenografts in nude mice. Cresyl violet staining of cell bodies visualizing the tumor development in two mice (A and B), as well as histological differences between tumor and normal brain tissue (C, D, and E). A) Brain section from mouse inoculated with 1 x 10^6 U-87 MG cells. B) Brain section from mouse inoculated with 5 x 10^5 U-87 MG cells. C) Tumor tissue at high magnification. D) Normal brain tissue at high magnification. E) Border between tumor and normal brain tissue at high magnification. A and B: 12.5x magnification. C, D, and E: 200x magnification.

4.2.2 Expression of GFAP

Brain sections from the two mice that developed intracranial tumors were also immunostained for GFAP to aid in characterization of tumor growth. GFAP is an intermediate filament of the cytoskeleton expressed by mature astrocytes and is therefore used as an astrocyte marker in the CNS. However, in astrocytomas the expression of GFAP progressively decreases with increasing malignancy, thereby differentiating astrocytic tumors from normal brain tissue. Immunohistochemical staining for GFAP demonstrated lack of expression in the U-87 MG tumor xenografts, while GFAP was abundantly expressed in surrounding normal brain tissue, revealing the tumors as unstained areas in the brain sections from the two mice (Figure 6A and B). The distribution of the unstained areas was consistent with the tumors observed in sections stained with cresyl violet, with a large, subcortical tumor in the brain of the mice inoculated with 1 x 10^6 U-87 MG cells (Figure 6A), and a smaller tumor with intraventricular spread in the brain of the mouse inoculated with 5 x 10^6 cells (Figure 6B). At high magnification, very few GFAP positive cells could be detected in the tumor area (Figure 6C). In contrast, highly GFAP reactive astrocytes with a star-like morphology were visualized within the normal brain tissue (Figure 6D). This distinctive expression pattern for GFAP generated a visible border between the tumor and

the normal brain tissue (Figure 6E). No unspecific staining was seen for negative control sections, where the primary GFAP antibody was omitted.

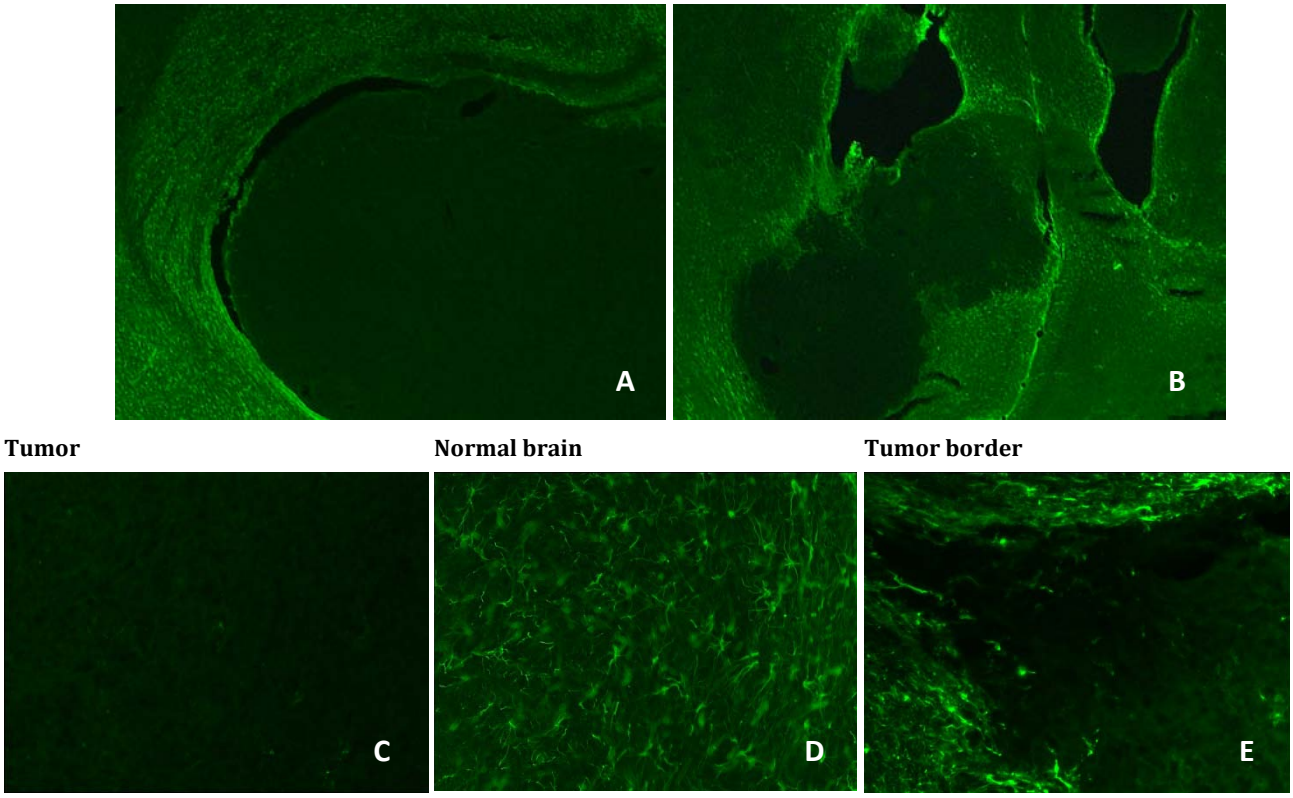

Figure 6. Expression of GFAP in U-87 MG tumor xenografts in nude mice. Immunohistochemical staining of GFAP visualizing the tumors as the unstained areas of the brain sections (A and B), as well as the lack of GFAP expression in tumor tissue (C) contrasted to the prominent GFAP expression in normal brain tissue (D), generating a visible border between the two (E). A) Brain section from mouse inoculated with 1 x 10^6 U-87 MG cells. B) Brain section from mouse inoculated with 5 x 10^5 U-87 MG cells. C) Tumor tissue at high magnification. D) Normal brain tissue at high magnification. E) Border between tumor and normal brain tissue at high magnification. A and B: 25x magnification. C, D, and E: 200x magnification.

4.2.3 Accumulation of Mouse Albumin

Immunohistochemical detection of mouse albumin was used to investigate the vascular permeability within the tumor area of the generated tumor xenografts. Albumin is a 69 kDa serum protein that is normally confined to the vascular space, however conditions with increased vessel permeability can permit the leakage of albumin and other macromolecules of the blood out into the extravascular space. Immunostaining of the brain tissue sections demonstrated some diffuse mouse albumin reactivity in the tumor tissue (Figure 7A), while in the normal brain tissue mouse albumin showed a vessel-like distribution (Figure 7B). In addition, the intensity of mouse albumin reactivity in the tumor was somewhat higher than within the normal brain tissue. Together this suggests some intratumoral accumulation of mouse albumin that might not be restricted exclusively to the vascular space. However, the intensity of mouse albumin immunostaining exhibited was low compared to background in both the tumor and normal brain tissue, complicating any interpretation of the staining patterns. Negative control sections only incubated with secondary antibody displayed a vague, randomly distributed, granulated staining (data not shown), resembling neither the pattern observed in the tumor nor in normal brain tissue.

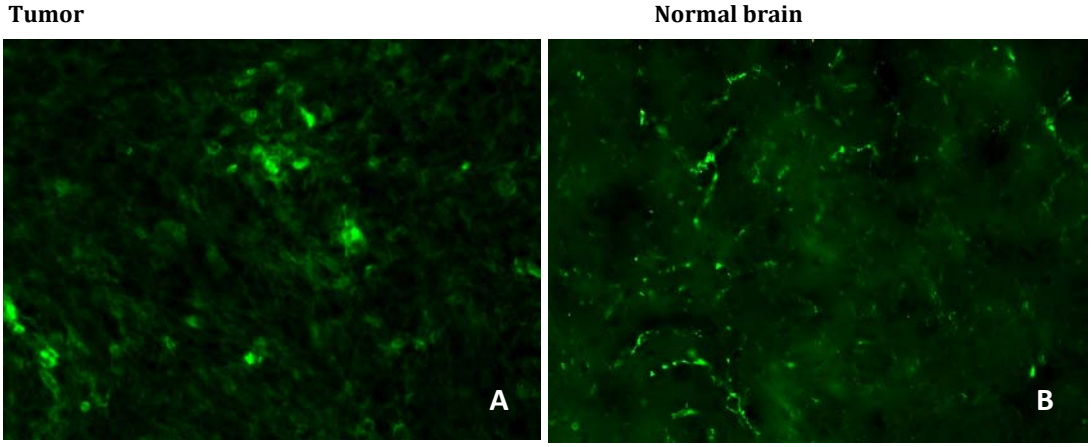

Figure 7. Accumulation of mouse albumin in U-87 MG tumor xenografts in nude mice. Immunohistochemical staining of mouse albumin vaguely showing a diffuse distribution in the tumor (A), and a vague vessel-like pattern in the normal brain tissue (B). A) Tumor tissue at high magnification. B) Normal brain tissue at high magnification. All images: 200x magnification.

4.2.4 Accumulation of Peroxidase

Vascular permeability in the tumor area was further studied by examining the intratumoral accumulation of peroxidase in one of the mice. 1 hour before euthanasia this mouse received an intraperitoneal injection of peroxidase, resulting fast uptake into the circulation and transport with the blood. As for mouse albumin, the circulating peroxidase was only able to transverse the blood-brain barrier and accumulate in areas of the brain with increased vascular permeability. Intravascular peroxidase was flushed out during perfusion fixation of the mouse, only retaining extravascular located peroxidase for reaction with DAB. Immunostaining for GFAP was used as counterstain to determine the localization of the tumor xenograft in the brain sections, visualizing tumor tissue as a large unstained area of the brain (Figure 8A). DAB staining of the same brain section revealed peroxidase activity in the central part of the depicted tumor (Figure 8B). At higher magnification, it was evident that the DAB staining predominantly was localized as small, demarcated areas of varying staining intensity, almost displaying a cell-like pattern (Figure 8C). Between some of the demarcated areas, a more diffuse staining of vague intensity could be seen. The tumor area also contained some small cells reacting strongly with DAB, distributed both as single cells and in clusters. To investigate the source of the peroxidase activity, brain sections from the other mouse that had not received any exogenous peroxidase were also reacted with DAB and counterstained for GFAP. Tumor distribution was identified based on the lack of GFAP reactivity (Figure 8D), and DAB staining of the same section now demonstrated peroxidase activity restricted to strongly reacting, small cells in a vessel-like pattern (Figure 8E and F). As erythrocytes are known to display endogenous peroxidase activity, the small, strongly positive cells observed in brain sections from both mice, most likely comprise residual erythrocytes in the blood vessels not flushed out during perfusion. Differences in vessel-like organization of the small, strongly staining cells between the two mice probably reflect variation in the completeness of erythrocyte wash out. In the second mouse, no extravascular areas of the tumor showed visible peroxidase activity (Figure 8E and F), supporting the view that the demarcated DAB stained areas observed in the brain of the mouse injected with peroxidase, indeed could be attributed to extravasation of intravascular peroxidase.

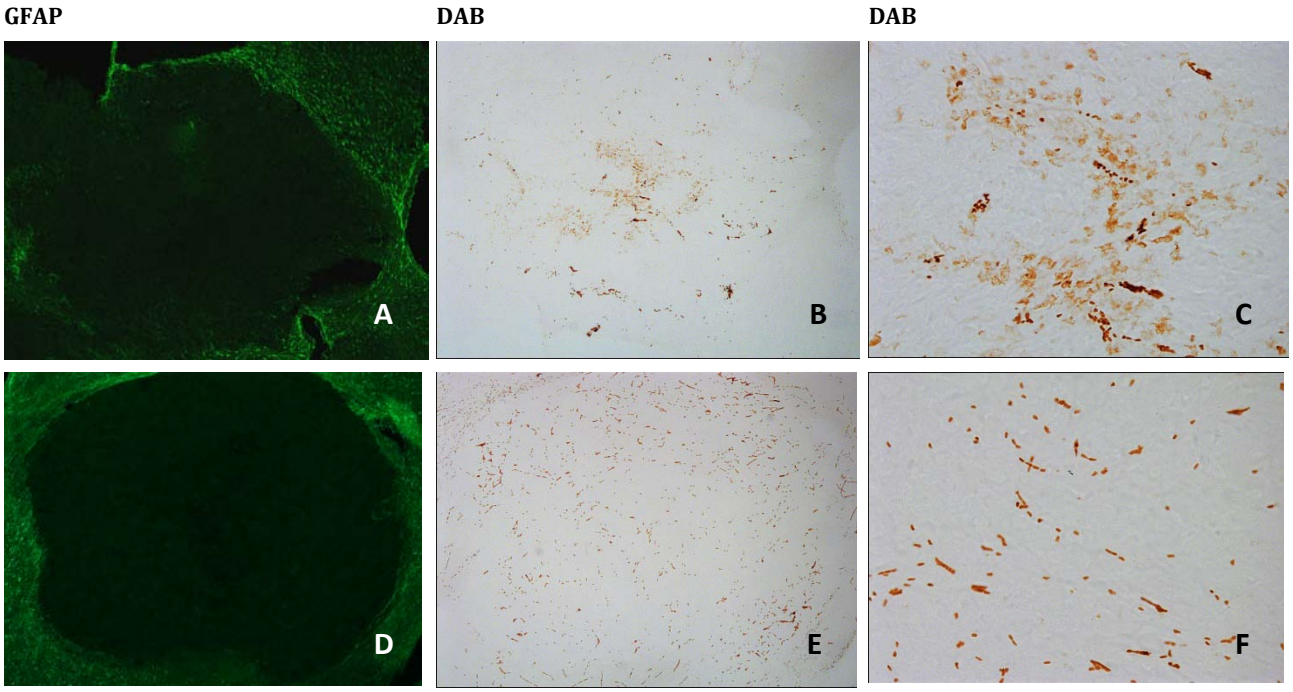

Figure 8. Peroxidase acitivity in U-87 MG tumor xenografts in nude mice with GFAP immunostaining as counterstain. Immunohistochemical staining of GFAP visualizing the tumors as the unstained areas of the brain sections (A and D), and DAB staining demonstrating extravasation of peroxidase in the tumor of a mouse injected with peroxidase prior to euthanasia (B and C), whereas only erythrocyte confined peroxidase activity could be observed in the tumor of a mouse receiving no exogenous peroxidase (E and F). A, B, and C) Brain section from mouse injected intraperitonenally with peroxidase 1 hour prior to euthanasia. D, E, and F) Brain section from mouse not injected with peroxidase. A and C) GFAP staining of tumor. B and E) DAB staining of tumor. C and F) DAB staining of tumor tissue at high magnification. A, B, D, and E: 50x magnification. C and F: 200x magnification.

4.2.5 Expression of EGFR and VCAM-1

The in vivo expression of the target molecules chosen for directing immunoliposomes to glioblastoma cells and tumor endothelial cells was investigated in the established U-87 MG tumor xenografts by immunocytochemistry. The used primary antibodies were the same as intended for liposomal targeting of these molecules.

Immunostaining for EGFR clearly demonstrated that expression was retained by the U-87 MG cells after in vivo implantation, demonstrating a more or less even level of expression in the whole tumor area (Figure 9A). As expected, no staining occurred outside the tumor, since Erbitux® specifically recognizes the human version of the EGFR. At higher magnification, the diffuse pattern of EGFR expression in the tumor tissue could be observed (Figure 9B). Negative control sections only incubated with secondary antibody displayed an unspecific, randomly distributed, vague granulated staining (data not shown), equally distributed in tumor and normal brain tissue.

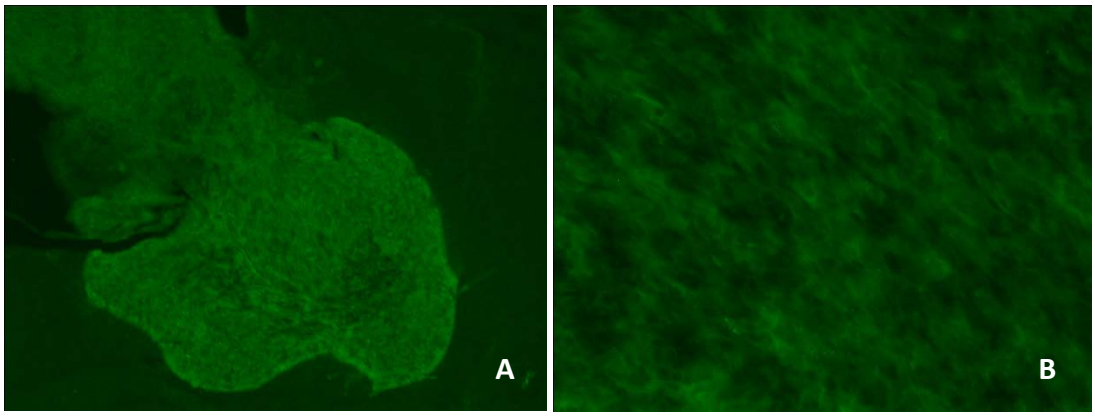

Figure 9. Expression of EGFR in U-87 MG tumor xenografts in nude mice. Immunohistochemical staining of EGFR showing an even level of expression throughout the tumor (A) in a diffuse pattern (B). (A) EGFR staining of tumor. B) EGFR staining of tumor tissue at high magnification. A: 25x magnification. B: 200x magnification.

In contrast, no widespread VCAM-1 expression could be detected neither within the tumor area nor in the normal brain tissue (Figure 10A). Only few isolated vessels located within the tumor were clearly VCAM-1 positive (Figure 10B). Vague, unspecific staining in a random, granular pattern could be seen both in stained sections and negative controls, where no primary antibody was added. Thus, only widespread intratumoral expression of the chosen cancer cell target EGFR could be confirmed in the U-87 MG tumor xenografts, whereas only scarce expression of the endothelial cell target VCAM-1 could be detected.

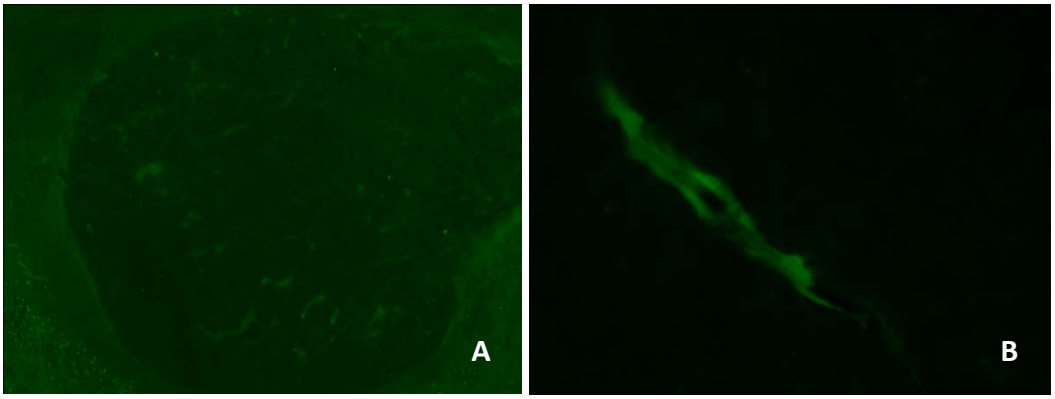

Figure 10. Expression of VCAM-1 in U-87 MG tumor xenografts in nude mice. Immunohistochemical staining of VCAM-1 showing lack of widespread expression within the tumor (A), and only few isolated tumor vessels clearly expressing VCAM-1 (B). (A) VCAM-1 staining of tumor. B) VCAM-1 staining of tumor tissue at high magnification. A: 25x magnification. B: 200x magnification.

4.3 Preparation and Characterization of Immunoliposomes

4.3.1 Characteristics of Prepared Liposomes

Determining the physical and chemical characteristics of liposomes is important as a measure of quality control and reproducibility of the prepared liposomes. Furthermore, knowing the basic characteristics of the liposomes will aid in interpretation of experimental results, since the liposome formulation greatly influences the in vitro and in vivo behavior. The prepared liposomes used for investigation of

the difference in cellular binding and uptake of targeted and untargeted liposomes were characterized with respect to particle size, zeta potential and protein/lipid ratio. The mean particle size, polydispersity, and zeta potential for the three different types of liposomes are given in Table 1. Unconjugated liposomes were prepared by the same technique as the immunoliposomes, but only included transfer of micelles without any coupled antibody. The resultant unconjugated liposomes had mean size of 115 ±3.22 nm and a low polydispersity, demonstrating a narrow size distribution of the liposomes. The mean size of the Erbitux®-liposomes was more than double the size of the unconjugated liposomes and with a broader size distribution. This large increase in size might not solely be attributed to the increase in size caused by conjugation of antibody molecules to surface, since previous experience with coupling of human serum IgG of comparable size only had increased liposomal size to between 180 and 200 nm (data not shown). Surprisingly, anti-VCAM-1-liposomes had a mean particle size and polydispersity resembling the size distribution of the unconjugated liposomes, possibly indicating lack of antibody conjugation. Little difference was observed in the zeta potential of unconjugated and Erbitux®-liposomes, both being slightly negative. However, the standard deviation of the zeta potential for the unconjugated liposomes was quite large due to significant variation between individual measurements, making any direct comparison difficult. In contrast to two other types of liposomes, the zeta potential of the anti-VCAM-1-liposomes was basically neutral.

	Particle size (nm)	**Polydispersity**	**Zeta potential (mV)**
Unconjugated liposomes	115.0 (±3.22)	0.071 (±0.011)	-23.5 (±7.64)
Erbitux®-liposomes	248.0 (±19.91)	0.218 (±0.021)	-25.7 (±0.283)
Anti-VCAM-1-liposomes	118.5 (±0.53)	0.064 (±0.009)	-2.65 (±0.078)

Table 1. Size and zeta potential of prepared liposomes. Unconjugated liposomes and anti-VCAM-1-liposomes displayed a narrow size distribution approximating 100 nm, whereas Erbitux®-liposomes were much larger with a mean size well above 200 nm and a wider size distribution. The zeta potential was slightly negative for both unconjugated liposomes and Erbitux®-liposomes, but in contrast the zeta potential of the anti-VCAM-1-liposomes was basically neutral. Particle size and polydispersity of the liposome suspensions were determined by dynamic light scattering and the zeta potential by laser Doppler electrophoresis. Each value was determined as the mean value of three independent measurements.

The protein concentration of the final liposome supspensions was determined by a commercially available modified Lowry assay. Human serum IgG was used for preparation of the standard curve in order to reduce signal variability from the content of aromatic amino acids in the standard compared to the protein of interest. Amines present in the liposomal lipids did not interfere with quantification of liposomal protein concentration, when the final liposome suspensions were diluted to a lipid concentration corresponding to a 1:5 dilution of unconjugated liposomes, reducing the lipid signal to the background level of the assay buffer. The phosphatidyl concentration of the final liposome suspensions was quantified using a commercial colorimetric assay, and the total lipid concentration was estimated from the phosphatidyl choline concentration, based on the fact that phosphatidyl choline constitutes approximately 65 mol% of the liposome lipids. The protein/lipid ratios demonstrated a far more efficient coupling of Erbitux® to the liposomes than VCAM-1 antibody (Table 2). Furthermore, the number of antibody molecules was estimated from the protein and lipid concentration, based on the assumption that a liposome approximating 100 nm in size consist of 100,000 phospholipid mole-

cules. This estimated a number 239 antibody molecules coupled per Erbitux®-liposome compared to only 40 antibody molecules per anti-VCAM-1-liposome (Table 2).

	µg protein/ µmol lipid	Antibody molecules per liposome
Erbitux®-liposomes	240	239
Anti-VCAM-1-liposomes	40	40

Table 2. Antibody coupling of prepared immunoliposomes. The coupling of Erbitux® to liposomes was far more efficient than coupling of VCAM-1 antibody, demonstrating a coupling efficiency 6 times higher for Erbitux® when comparing the amount of conjugated protein per µmol lipid and the number of antibody molecules per liposome. The protein/lipid ratio was calculated from the determined protein and lipid concentration of the final liposome suspensions. The number of antibody molecules per liposome was estimated based on the determined protein and lipid concentration of the final liposome suspensions, and the assumption that a liposome approximating 100 nm in size consist of 100,000 phospholipid molecules.

4.4 In Vitro Cellular Binding and Uptake of Liposomes

4.4.1 Fluorescencence Microscopy of Cellular Binding and Uptake of Liposomes

In vitro cellular binding and uptake of immunoliposomes targeted to U-87 MG cells or bEnd.3 cells compared to unconjugated liposomes were examined by fluorescence microscopy of cells incubated with green fluorescent liposomes. The antibodies used for the preparation of immunoliposomes were the same as previously used for successful immunostaining of EGFR and VCAM-1 and the characteristics of the resulting immunoliposomes are given in section *4.3.1*.

After incubation with liposomes for 2 hours at 37 °C, U-87 MG cells showed no visible uptake or binding of liposomes of unconjugated liposomes (Figure 11A-C). In contrast, Erbitux®-liposomes were readily taken up by the cells during this time period and could be detected as a granulated pattern of cytoplasmic green fluorescence of cells with nuclear DAPI staining (Figure 11D-E). This demonstrates that targeting of liposomes to the EGFR using the Erbitux®-antibody indeed induces specific uptake of the liposomes by U-87 MG cells. The green smear visible in Figure 11E and F is a green fluorescent filament, of which numerous were present in all wells co-stained with DAPI, but none could be observed in wells without DAPI staining. Thus, the filaments might originate from precipitation of DAPI during staining.

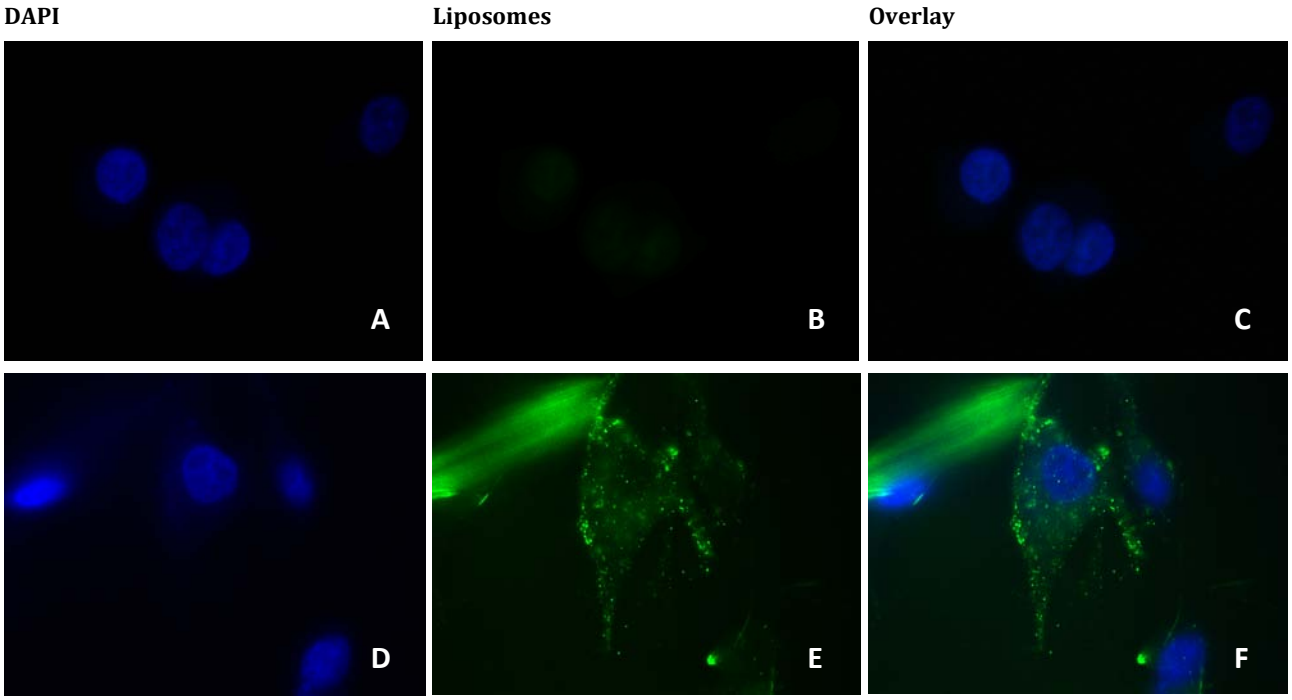

Figure 11. Cellular uptake of green fluorescent liposomes by U-87 MG cells. No cellular uptake of unconjugated liposomes was observed after incubation for 2 hours at 37 °C (A-C), whereas specific uptake of Erbitux®-liposomes was demonstrated by cytoplasmic distribution of green fluorescent liposomes in the cells (D-F). A-C) U-87 MG cells incubated with unconjugated liposomes. D-F) U-87 MG cells incubated with Erbitux®-liposomes. A and D) DAPI staining of cell nucleus. B and E) Cellular distribution of green fluorescent liposomes. C and F) Overlay of column 1 and 2. All images: 1000x magnification.

The cellular uptake of the vascular targeted immunoliposomes was investigated using bEnd.3 cells activated with 50 ng/ml TNF-α for 4 hours. Like for the U-87 MG cells, no cellular uptake or binding of unconjugated liposomes could be detected microscopically for the bEnd.3 cells after 2 hours of incubation at 37 °C (Figure 12A-C). However, in contrary to the expected, the anti-VCAM-1-liposomes displayed no visible cellular accumulation or binding, when incubated with activated bEnd.3 cells (Figure 12D-F). No evidence therefore indicate that antibody binding to the VCAM-1 promote specific uptake of liposomes by bEnd.3 cells.

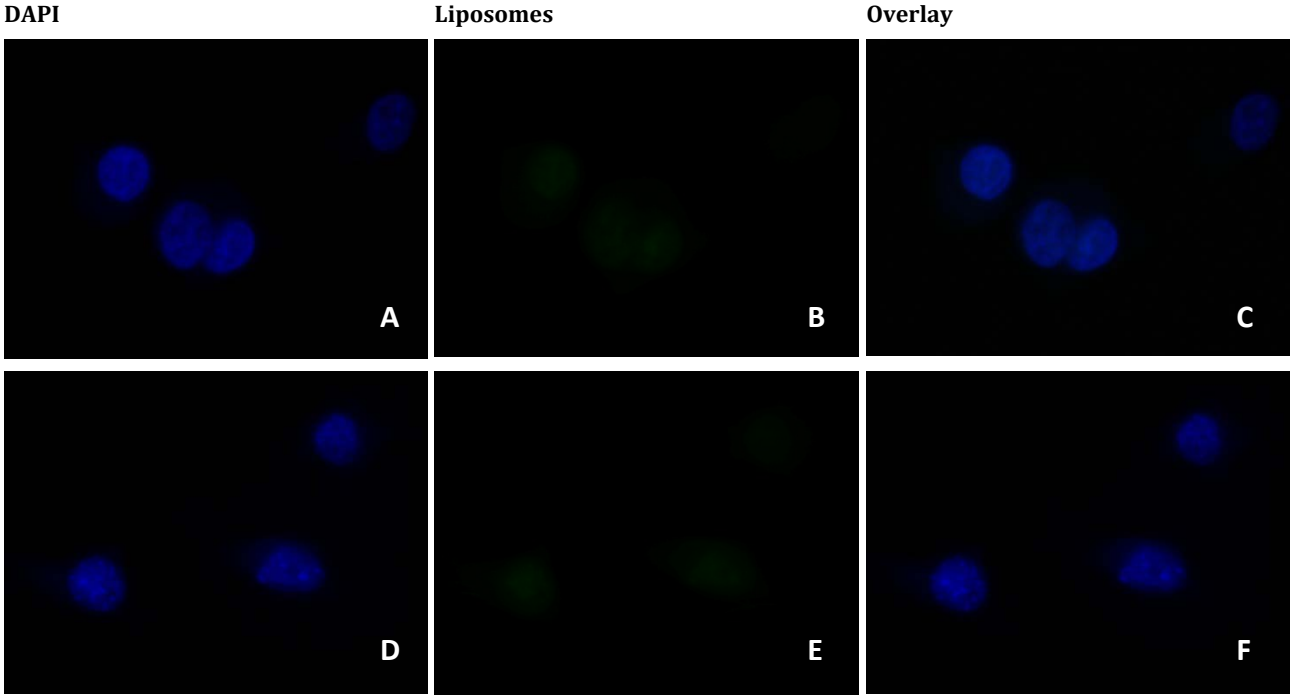

Figure 12. Cellular uptake of green fluorescent liposomes by bEnd.3 cells activated with 50 ng/ml TNF-α for 4 hours. No cellular uptake of neither unconjugated liposomes (A-C) nor anti-VCAM-1-liposomes (D-F) was observed after incubation for 2 hours at 37 °C. A-C) bEnd.3 cells incubated with unconjugated liposomes. D-F) bEnd.3 cells incubated with anti-VCAM-1-liposomes-liposomes. A and D) DAPI staining of cell nucleus. B and E) Cellular distribution of green fluorescent liposomes. C and F) Overlay of column 1 and 2. All images: 1000x magnification.

4.4.2 Flow Cytometer Analysis of Cellular Binding and Uptake of Liposomes

Cellular binding and uptake of unconjugated liposomes and immunoliposomes were quantified by flow cytometer analysis after incubation for 2 hours at 37 °C for both U-87 MG cells and bEnd.3 cells. For each cell type, the cell population was identified based on cell size and granularity of cells without liposomes, and only cells corresponding to this population were included in analysis of the different samples. Autofluorescence of cells not incubated with liposomes was also determined for each cell type, and in order to subtract this background fluorescence from the liposome signal a gate was established, maximally including 1 % of autoflourescent cells, and only fluorescence intensity above this gate was included in analysis.

For the U-87 MG cells, no difference in cellular fluorescence of cells without liposomes (Figure 13A) and cells incubated with unconjugated liposomes (Figure 13B) was detected by flow cytometric analysis. Less than 1 % of the cells with unconjugated liposomes displayed fluorescence above the background level and no difference in mean fluorescence intensity was seen when compared to cells without liposomes (Table 3Table 3). In contrast, cells incubated with Erbitux®-liposomes demonstrated significantly higher fluorescence (Figure 13C), reflecting cellular binding and uptake of the targeted liposomes. Approximately 85 % of U-87 MG cells exhibited fluorescence above the background level and a significantly higher mean intensity of fluorescence than the cells incubated with unconjugated liposomes (Table 3). Thus, it was demonstrated that Erbitux®-liposomes were specifically bound and internalized by the majority of U-87 MG cells.

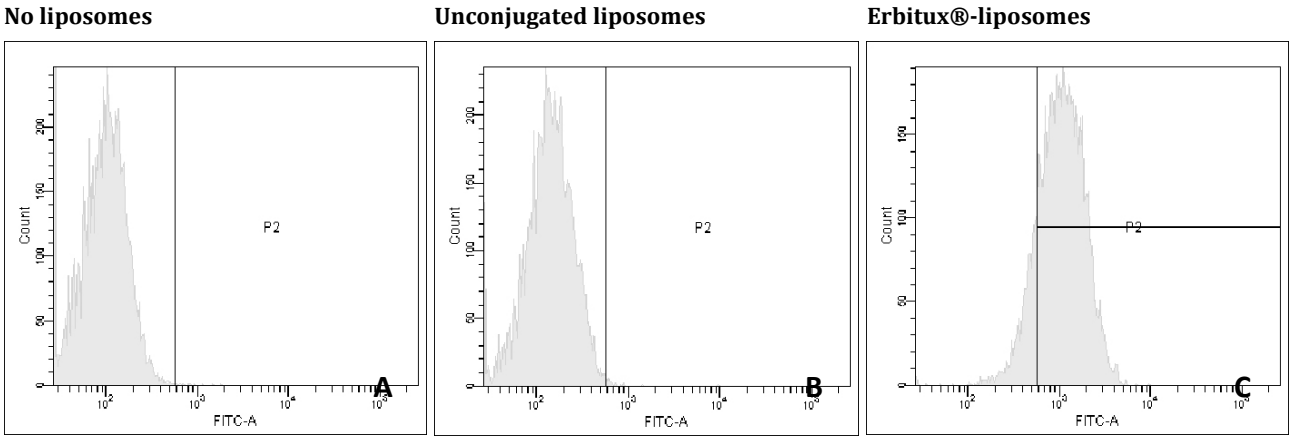

Figure 13. Flow cytometric analysis of cellular binding and uptake of green fluorescent liposomes by U-87 MG cells. Cellular fluorescence of cells incubated with unconjugated liposomes for 2 hours at 37 °C (B) did not differ from background fluorescence of the cells (A), whereas Erbitux®-liposomes demonstrated specific binding and uptake by a large fraction of the cells (C). A) Cells not incubated with liposomes. B) Cells incubated with unconjugated liposomes. C) Cells incubated with Erbitux®-liposomes.

	Positive cells	Mean intensity
No liposomes	1 %	1,052
Unconjugated liposomes	0.3 %	1,019
Erbitux-liposomes	84.8 %	1,357

Table 3. Percentage of positive cells and mean fluorescence intensity of U-87 MG cells determined by flow cytometric analysis. The percentage of positive cells and the mean cellular fluorescence intensity did not differ from background values after incubation with unconjugated liposomes for 2 hours at 37 °C, whereas approximately 85 % of all cells demonstrated significantly higher fluorescence from the specific uptake of Erbitux®-liposomes. Positive cells: Percentage of cells above background level of fluorescence. Mean intensity: Mean green fluorescent intensity of cells above background.

To stimulate the cellular expression of VCAM-1 and promote uptake of targeted liposomes, the bEnd.3 cells were activated with 50 ng/ml TNF-α for 4 hours prior to incubation with liposomes. However, no uptake of neither unconjugated nor anti-VCAM-1 liposomes could be detected by flow cytometric analysis, when comparing the cellular fluorescence to the background level (Figure 14A-C and Table 4). Thus, antibody targeting of VCAM-1 did not seem to increase the cellular uptake of liposomes.

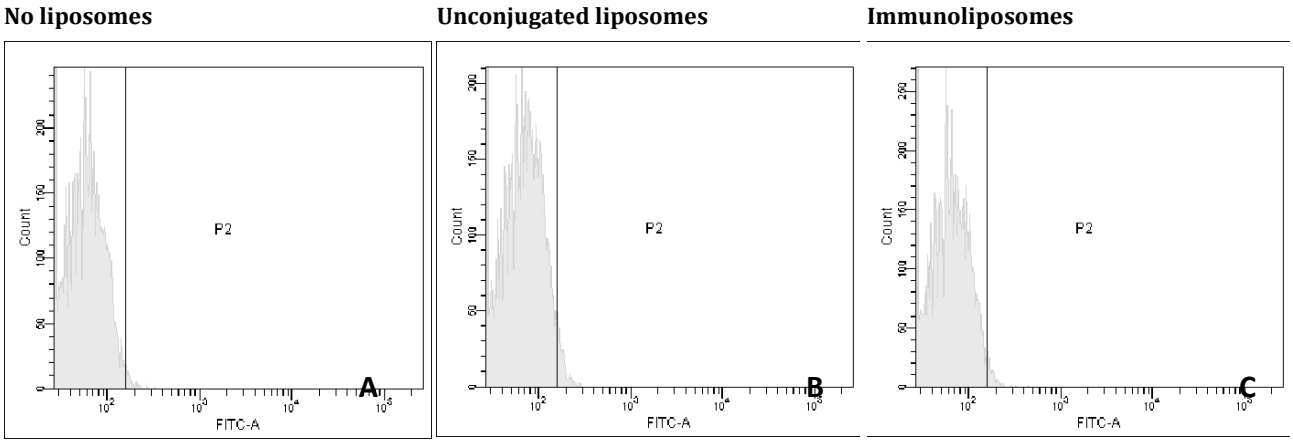

Figure 14. Flow cytometric analysis of cellular binding and uptake of green fluorescent liposomes by bEnd.3 cells activated with 50 ng/ml TNF-α for 4 hours. Cellular fluorescence of cells incubated with unconjugated liposomes (B) or anti-VCAM-1-liposomes (C) for 2 hours at 37 °C did not differ from background fluorescence of the cells (A). A) Cells not incubated with liposomes. B) Cells incubated with unconjugated liposomes. C) Cells incubated with anti-VCAM-1-liposomes.

	Positive cells	Mean intensity
No liposomes	1	180
Unconjugated liposomes	3.2	181
Anti-VCAM-1-liposomes	1.7	183

Table 4. Percentage of positive cells and mean fluorescence intensity of bEnd.3 cells determined by flow cytometric analysis. The percentage of positive cells and the mean cellular fluorescence intensity did not differ from background values after incubation with neither unconjugated liposomes nor anti-VCAM-1-liposomes for 2 hours at 37 °C. Positive cells: Percentage of cells above background level of fluorescence. Mean intensity: Mean green fluorescent intensity of cells above background.

4.5 In Vivo Biodistribution of Liposomes

4.5.1 Fluorescence Microscopy of Tissue Sections

In order to study the in vivo stability of the liposomal formulation and develop an appropriate method for assessing the biodistribution of fluorescent liposomes two mice were injected intravenously with unconjugated liposomes. 24 hours later a blood sample were obtained before terminating the mice by transcardial perfusion and the mouse brains were removed together with organs of relevance to liposomal clearance or liposome associated side effects. Fixated tissue sections from the removed organs were examined for liposome accumulation by fluorescence microscopy and compared to control sections from a rat that had not received any liposomes. In general, the background fluorescence of the fixated sections was quite high, making it difficult to identify accumulated liposomes. Therefore microscopic examination yielded no conclusions regarding biodistribution of injected liposomes in most of the organs. However, in the liver and spleen of the two nude mice green fluorescence could clearly be observed, when compared to control rat sections. Liver sections from the two nude mice showed accumulation of green fluorescent liposomes in what appeared to be single cells, randomly distribution throughout the liver tissue (Figure 15A and B), whereas no localized fluorescence was observed in the

control liver sections (Figure 15C). In the spleen, green fluorescent liposomes was primarily localized in distinct areas (Figure 15D and E), and the intensity was clearly higher than the corresponding background fluorescence of control sections (Figure 15F).

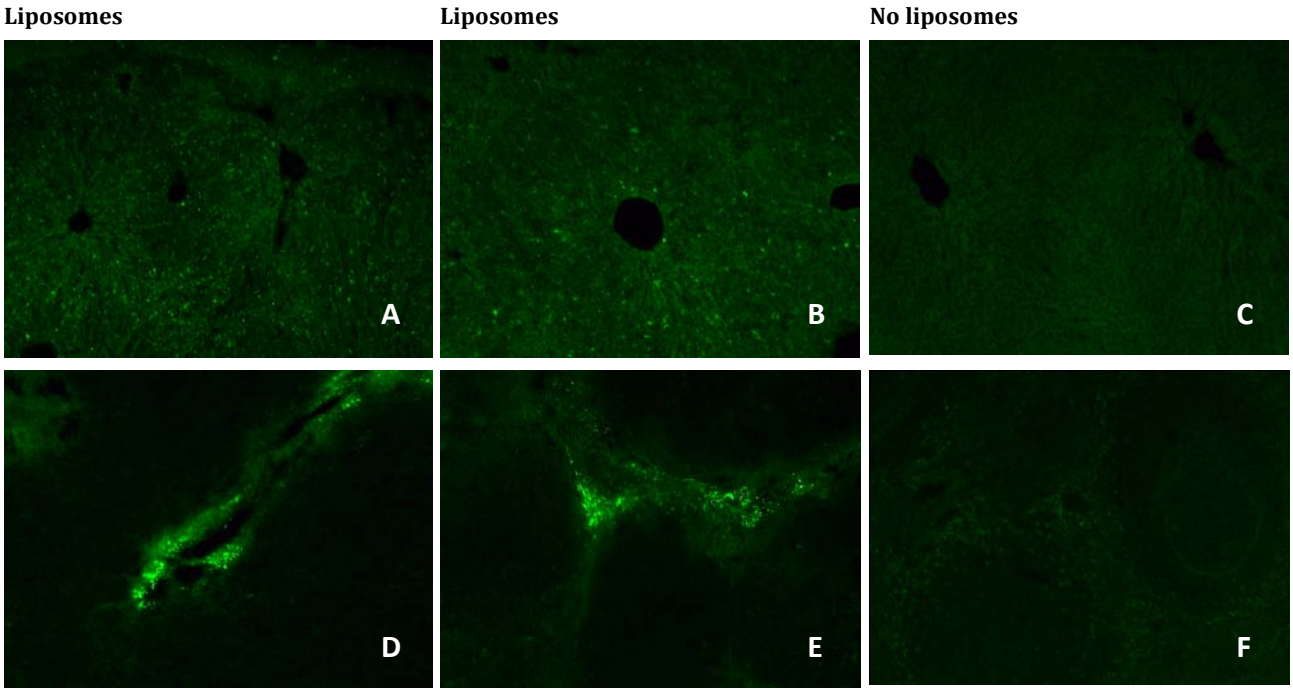

Figure 15. Distribution of unconjugated green fluorescent liposomes in liver and spleen sections. Accumulation of unconjugated liposomes could be observed in cells scattered throughout the liver (A and B) and in the distinct areas of the spleen (D and E) 24 hours after intravenous injection in two nude mice, when compared to liver (C) and spleen (F) sections from a rat receiving no liposomes. A-C) Liver sections. D-F) Spleen sections. A, B, D, and E) Sections from two different mice 24 hours after injection with unconjugated green fluorescent liposomes. C and F) Control sections from a rat receiving no liposomes. All images: 100x magnification.

4.5.2 Fluorescence Spectroscopy Analysis of Tissue Homogenates

In order to determine the tissue accumulation of fluorescent liposomes quantitatively, fresh frozen samples of the removed organs were thoroughly homogenized for fluorescence spectroscopy. After measuring fluorescence intensity of the tissue homogenates, obtained values were normalized by the amount of homogenized tissue to enable comparison of the samples. The background levels of fluorescence in the different tissues were assessed by analyzing homogenized rat tissue. However, due to time constraints, only brain, liver, spleen, and blood homogenates from one mouse and corresponding control samples have been analyzed so far. Samples of each tissue were homogenized in two different buffers, to investigate the effect of including mild detergents herein, but no consistent difference between the two buffers could be observed in fluorescence intensity. The results from analysis of samples homogenized in detergent-containing buffer are listed in Table 5. All samples from the mice injected with liposomes displayed higher fluorescence than the background fluorescence of the associated control samples, indicating that after 24 hours of circulation liposomes had accumulated in the brain, liver and spleen, and was still present in the blood. Compared to the brain samples, the observed difference between liposome containing sample and control for both the liver and spleen was more than three times larger, suggesting a higher accumulation of unconjugated liposomes in these tissues. Fluorescence intensity of the analyzed blood plasma was much higher for both animals than for any of

the analyzed tissue homogenates. However, even though equivalent volumes of plasma and tissue homogenate were analyzed, the obtained fluorescence intensities cannot be directly compared, since serum was analyzed directly without further homogenization and therefore not diluted to the same extent as the homogenates. Overall, fluorescence spectroscopy indeed seems to be a feasible method for detecting the extent of liposomal accumulation in different tissues in vivo, but further analysis will have to confirm this for the remaining organs of interest.

	Brain	Liver	Spleen	Blood
Unconjugated liposomes	518*	1739	1310	200165
No liposomes	220	690	343	115495
Difference	298	1049	967	184670

Table 5. Arbitrary flourescence intensity of tissue homogenates and blood serum. All samples from the nude mouse injected with liposomes 24 hours earlier clearly exhibited a higher level of fluorescence than control rat samples, and it seemed that liposomes accumulated more readily in the liver and spleen than in the intracranial tumor of the nude mouse. *) Arbitrary fluorescence intensity of tumor tissue. The arbitrary fluorescence intensities correspond to 100 µl of tissue homogenate and 100 µl of blood serum. All tissue homogenate fluorescence intensities were normalized with the amount of homogenized tissue. Fluorescence intensities were determined at an excitation wavelength of 457 nm and an emission wavelength of 532 nm.

5 DISCUSSION

5.1 Tumor Growth and Vascular Permeability of Intracranial U-87 MG Tumor Xenografts

One of the primary aims of this thesis was to establish an intracranial animal model of human glioblastoma multiforme and characterize this model with respect to tumor growth and vascular permeability. For this purpose, the immortalized human glioblastoma cell line U-87 MG was chosen, based on the fact that it is one of the most widely used and well-characterized immortalized glioblastoma cell lines both for in vitro studies and in vivo implantation. To investigate the tumorigenic potential in vivo of U-87 MG cells, two different doses of U-87 MG cells was inoculated into the striatum of three immunodeficient mice, and within three weeks two out of the three mice developed signs of intracranial tumor growth, assessed by a significant, progressive loss of weight. Histological analysis revealed a very large tumor in the brain of the mouse injected with the largest bolus of cancer cells, and this mouse was in fact also the mouse that displayed significant weight loss first. However, only a few days later the mouse inoculated with half as many cancer cells also started losing weight, even though the size of this tumor was much smaller. Using a small animal stereotactic apparatus, the needle of the syringe containing U-87 MG cells was targeted to the striatum, but due to extensive growth and local invasion of the established tumors, it was difficult to assess the achieved accuracy of their location. Furthermore, the tumor in the brain of the mouse inoculated with the smallest dose of cancer cells, extended almost into the cortical area, possibly reflecting the growth of cancer cells that had ascended through the track of the needle after its removal. In future experiments, this might be limited by the use of a syringe with a smaller needle. Overall, it might be advantageous to examine the exact location of tumor development at an earlier time point after cancer cell implantation. Based on the experiences from this experiment, the smallest dose of 500,000 cancer cells was chosen as a sufficient dose for establishing intracranial U-87 MG xenografts in nude mice. Using this protocol, the three mice used for investigating of liposomal biodistribution were inoculated with cancer cells, and the success rate of tumor development was again two out of three as assessed by weight loss and macroscopic examination of brain sections.

Compared to published studies using intracranial implantation of U-87 MG cells in nude mice as a tumor xenograft model, our observations in general correlated well with reports of time to visible manifestations of tumor development and the size of the developed tumors (147, 149, 156, 157). For example, two studies demonstrated a median survival of 21 days (158) and between 21-32 days in a series of experiments (159) for untreated nude mice inoculated intracranially with 500,000 U-87 MG cells. This fits well with time points to mouse euthanasia due to loss of more than 20 % of baseline weight in our experiments. In addition, Laccabue et al 2001 (159) stated that the only observed manifestation of tumor growth was weight loss, which was also the case for the majority of the mice included in our experiments. However, our rate of tumor development was much lower than their rate of 100 % success after injection of 500,000 U-87 MG cells. One major reason for this difference is probably that the nude mice used in the study by Laccabue et al were only 9 weeks old at the time of cancer cell inoculation, compared to our mice being 6-10 months old, and it is well-established that the success rate for tumor development in nude mice decreases significantly with age (144). In further experiments mice of maximally 2-3 months of age will therefore be used in order to gain a higher success rate of tumor xenograft development.

Vascular permeability of the vessels within U-87 MG tumor xenografts was investigated by visualizing the distribution of intratumoral peroxidase activity and mouse albumin. Compared to healthy

brain tissue some evidence of increased accumulation of both these molecules in the tumor area could be observed, which might be interpreted as increased permeability of the tumor vessels. Diffuse DAB staining primarily occurred in the central areas of the tumor tissue, possibly indicating increased vascular permeability being confined to the tumor center. However, it was difficult to assess in which compartment of the tumor the peroxidase and albumin accumulation had occurred. Counterstaining with a nuclear stain such as DAPI or Hoeschst and staining with a vessel markers such as CD31 (platelet endothelial cell adhesion molecule-1) or von Willibrand factor might be helpful in confirming the extravascular location of the accumulated peroxidase and mouse albumin. If vascular permeability indeed is present in the tumor xenografts, it would be interesting to investigate the molecular cut-off size of extravasating molecules, since immunoliposomes targeting the U-87 MG cells would accumulate in the tumor via the EPR effect. The size of the liposomes should therefore be guided by the size of the existing pores. Even though it is generally accepted that widespread angiogenesis occurs in U-87 MG xenografts, possible effects on vascular permeability and fenestrations have not been widely investigated. However, one study has demonstrated vascular permeability of intracranial tumors derived from implanted U-87 MG cells using gadolinium-DTPA contrast magnetic resonance imaging. Following administration of the contrast agent, imaging showed hyperintense enhancement of the tumor area, indicating tumor vessel permeability since gadolinium-DTPA only can extravasate into the interstitial space, when the blood-brain barrier is disrupted. (160) In addition, two studies investigated the vascular characteristics of implanted pieces of subcutaneously grown U-87 xenografts in an intracranial window. Using this model vascular permeability to fluorescently labeled BSA was demonstrated (161), as well as a tumor vessel pore cut-off size of approximately 100 nm (119). Thus, accumulating evidence show that intracranial U-87 MG xenografts indeed exhibit vascular permeability, but to achieve efficient intratumoral accumulation liposome size might need to be reduced to less than 100 nm.

5.2 In Vitro and In Vivo Target Expression

The expression of chosen targets for liposomal targeting was investigated both in vitro and in vivo for model systems of glioblastoma multiforme. The cancer cell target, EGFR, was clearly expressed by U-87 MG cells both in culture and after in vivo implantation, and therefore seems to be a good option for liposomal targeting of cancer cells. However, in glioblastoma patients EGFR expression is often accompanied by gene amplification and rearrangement. In comparison, the U-87 MG cell line only express modest levels of wild type EGFR (145, 162), since primary glioblastoma cells rapidly loose gene amplification and rearrangement, when cultured in vitro (158). VCAM-1 was chosen as the endothelial cell target of glioblastoma multiforme, based on success with vascular targeting of immunoliposomes using this molecule in other animal models of human cancers (79). The immortalized murine brain endothelial cell line, bEnd.3, was used as the in vitro equivalent of the host vessels that extend into the tumor xenograft. To induce an inflammatory condition, mimicking the in vivo tumor environment, the cells were treated with 50 ng/ml TNF-α for 4 hours. TNF- α is a cytokine, which is known to induce expression of several cell adhesion molecules, including VCAM-1 on endothelial cells (163). The specific setup was chosen based on the observed expression of VCAM-1 and practical issues, combined with the desire to limit the amount of added TNF-α and time of incubation, since this cytokine can be highly toxic to endothelial cells (164). In the tumor xenografts, only scarce expression of VCAM-1 was detected, and this molecule should therefore be revised as a tumor endothelial target, at least in this specific model of glioblastoma multiforme. In fact, the expression pattern of VCAM-1 as well as other leukocyte adhesion molecules in tumors is known to vary with different tumor types and vary locally

within the specific tumor lesion (135, 138). The differential expression have been suggested to play a role in tumor immune escape, since the orderly expression of adhesion molecules involved in leukocyte diapedesis must be strictly controlled to result in successful transendothelial migration (133). Targeting of immunoliposomes to VCAM-1 have been done successfully in tumor xenografts of other cancer types, but no existing literature have demonstrated widespread expression of this molecule neither in animal models of glioblastoma multiforme, nor in tissue samples obtained from patients.

5.3 Properties of Prepared Liposomes

The physical characteristics of liposomes are important determinants of their behavior in vitro and in vivo and must therefore be carefully considered when preparing liposomes for cancer targeting. The size of liposomes is an important determinant of the in vivo tissue distribution, accumulation in tumor tissue due to ERP effect, and as well as the circulation time. The observed size of 110-120 nm with a narrow size distribution for the prepared unconjugated liposomes correlates well with the size obtained by extrusion through 0.1 µm polycarbonate filters in published studies (128, 130, 165). However, antibody conjugation when using a lipid composition similar to the liposomes prepared in the work of this thesis was in general only reported to increase size by 10 nm (60, 166, 167). This is much less than observed increase between 50-100 nm during conjugation of Erbitux and during the optimization of the protocol for conjugation of IgG. The unexpected large increase in size of the liposomes might be caused by the aggregation of preformed liposomes, or by cross-linking of one antibody to several micelles, leading to cross-linking of liposomes during micelle transfer of the conjugated antibodiesLiposomes composed of a lipid composition comparable to the liposomes investigated in this thesis are generally slightly negative. The measured zeta potential for unconjugated liposomes and Erbitux®-liposomes fits well with reported zeta potentials for similar liposomal preparations (167). However, for some reason the zeta potential of the anti-VCAM-1-liposomes was almost neutral. A zeta potential of this value have not been observed before, when preparing liposomes of this lipid composition.

The calculated antibody coupling efficiency for the Erbitux®-liposomes was very high compared to the achieved antibody coupling reported by others using the micelle post insertion technique, in general reporting between 25-40 µg of antibody per µmol lipid (143). In contrast, the calculated amount of conjugated antibody for the anti-VCAM-1-liposomes resembled the coupling efficiencies reported by others. The amount of conjugated antibody and the number of antibody molecules per liposome were calculated from quantified protein and phosphatidyl choline concentrations of the final liposome suspensions. The prepared protein standard curve displayed perfect linearity, whereas several of the phosphatidyl choline standards clearly were divergent from the obtained standard curve. The resulting lack of precision might lead to under or over estimation of the total lipid content of the liposome suspensions, severely biasing the calculated protein-to-lipid ratios. Nevertheless, the in vitro cellular uptake study confirmed that the conjugated amount of Erbitux® indeed was sufficient to induce specific uptake of the liposomes by EGFR-expressing cells, while the conjugated VCAM-1 antibody seemed insufficient to induce liposome internalization by VCAM-1 expressing cells. An explanation for the variation in antibody conjugation might be the large difference in concentration of the two antibodies. After upconcentration of SATA-modified antibody, the VCAM-1 antibody was 20 times less concentrated than Erbitux®, due to an initial concentration of only 0.5 mg anti-VCAM-1 antibody per ml and a minimal concentration value of approximately 1 ml. When adding the corresponding molar ratio of micelles to the activated antibodies, the conjugation reaction will progress much more effectively if the protein to be coupled is highly concentrated. An moderate antibody concentration for in vivo cancer targeting has proven most advantageous, since this coupling balances the need for a high

target binding affinity and the need for prolonged circulation of the immunoliposomes. An approach to achieve higher coupling efficiency, while retaining a long half life in vivo is the use of antibody fragments as targeting agents instead of whole antibodies. Antibody fragments lack the Fc region and therefore the immunoliposome recognition and uptake by the RES occurs more slowly. Furthermore, fab fragments contain an inherent thiol group, liberated by cleaving the disulfur bridge to the constant part of the antibody. The thiol group can be utilized for coupling to maleimide, eliminating the need for SATA-modification of the targeting agent and thereby improving control over liposomal orientation and reducing the risk of cross-linking.

5.4 In Vitro Cellular Binding and Uptake of Liposomes

Specific uptake of Erbitux®-liposomes by U-87 MG cells in vitro was confirmed by both fluorescence microscopic investigations and flow cytometric analysis. In agreement with these results, Mamot and colleagues also showed specific uptake of liposomes conjugated with Erbitux® antibodies or fragments by U-87 MG cells (128). Here, fluorescence microscopy revealed extensive internalization and cytoplasmic accumulation of immunoliposomes in cultured cells after incubation at 37 °C for 2 hours with liposomes, followed by removal of unbound liposomes and growth for 2 hours without liposomes. In further studies, these immunoliposomes were also demonstrated to display significant intracellular accumulation in U-87 MG cells of subcutaneous tumor xenografts as well as improved therapeutic effects of doxorubicin-loaded immunoliposomes compared to untargeted liposomes and free drug (59). Overall, experiments performed with the Erbitux®-liposomes in this thesis provides proof of principle that the conjugation of antibody to liposomes through the developed post insertion protocol in fact can induce specific cellular uptake of prepared immunoliposomes. However, the protocols used in the work of this thesis did not distinguish between cell surface binding of liposomes and internalization, since flow cytometer analysis measures the total cell fluorescence and it is difficult to distinguish between true cytoplasmic and surface bound liposomes by standard fluorescence microscopy. Surface bound liposomes can be removed by washing cells with citrate buffer before performing flow cytometer analysis and thereby only the internalized fraction of cell bound liposomes is measured. In contrast, the fraction of cell surface associated liposomes can be determined as the difference in cellular fluorescence before and after washing with citrate buffer.

No cellular uptake of anti-VCAM-1-liposomes was observed by fluorescence microscopy or flow cytometer analysis. Since the bEnd.3 cells demonstrated expression of VCAM-1 at a significant level after TNF-α treatment and the used antibody previously have been applied for directing cellular uptake of liposomes (79), the lack of immunoliposome uptake probably reflected an insufficient amount of coupled antibody to the liposomes. Thus, further investigations will need to reveal if conjugation of more antibody to the liposomes induce specific cellular uptake.

5.5 In Vivo Biodistribution of Liposomes

After identification of suitable targets and proof of principle that immunoliposomal targeting hereof induce specific cellular uptake, the next step is to investigate the liposomal behavior in vivo. Therefore two methods for assessing the tissue distribution of fluorescent liposomes were investigated. Microscopic analysis revealed inconclusive results for most of the investigated tissues, due to a high background level of fluorescence of the fixated tissues and only in the liver and spleen liposomal fluorescence could be distinguished from the background signal. In the liver, liposomes exhibited a widespread pattern of accumulation, mimicking the liposomal pattern observed by other research groups, proposed to be consistent with the distribution of inherent macrophages, the Kuppfer cells. In the

spleen, liposomes seemed to accumulate in the distinct areas, consistent with the liposome uptake by macrophages of the RES. Counterstaining of tissue sections with markers against macrophages could aid in confirming such speculations. Fluorescence spectroscopy of tissue homogenates also indicated significant uptake of liposomes by the spleen and liver, at least when compared to brain tissue. Thus it seems plausible that fluorescence spectroscopy can be used to determine tissue accumulation of fluorescent liposomes, regardless of background fluorescence of the homogenized tissue. However, both methods require some optimization prior to further use. It might be advantageous to investigate sections of fresh, frozen tissue by fluorescence microscopy, to minimize fixation induced autofluorescence. Florescence spectroscopy determination of liposome accumulation also requires some optimization, especially with respect to intersample comparability. A higher degree of intersample comparability would enable quantification of nmol lipid per sample of tissue homogenate from a liposome standard curve and relate this to the amount of homogenized tissue to calculate the percentage of injected liposome dose that has accumulated in each organ.

5.6 Future Perspectives

So far, immunoliposomes for use in targeted cancer therapy have solely been investigated in the preclinical setting. Obtained results certainly provide a promise that in the future this drug carrier system could achieve more specific and less toxic clinical delivery of a wide variation of anticancer drugs in cancers such as glioblastoma multiforme, where currently available therapy lacks efficiency. However, for liposome-based anticancer therapy to display maximal effect and minimal side effects, it requires identification of specific target molecules and appropriate drugs to be delivered. Targeting of several distinct tumor compartments by combining immunoliposomes of different targeting specificities could aid in directing drugs to a larger proportion of the tumor. It can be difficult to achieve a sufficient drug delivery using only one targeting agent due to the heterogeneous molecular profile of both cancer cells and tumor endothelial cells. In addition, applying liposomes directed to a single target probably could result in development of cellular resistance mechanisms, as observed in the clinical setting when administering molecular targeted drugs as monotherapy. Simultaneous liposomal drug delivery to several distinct cell populations within the tumor, such as cancer cells and tumor endothelial cells, as well as putative cancer stem cells, might generate synergistic therapeutic effects and minimize drug resistance.

An advantage of using the post insertion technique for preparation of cancer targeted immunoliposomes is that this technique has the potential for development of a “mix and match” strategy. Based on the molecular profile of a specific tumor, patient-specific antibodies can be conjugated to commercially available untargeted liposomes, tailoring drug-loaded immunoliposomes to the tumor cells. If an arsenal of liposomes containing different therapeutic molecules is made available, this approach allow not only for tailoring the targeting antibody but also the active drug to the molecular profile of the target cell. Thus, based on the molecular characteristics of the different cell populations within a specific tumor, immunoliposomes that target a highly expressed molecule and contain a drug of anticipated effect can be prepared specifically for the chosen target cell population. In the clinical setting, this allows application of highly “personalized”, multitargeted immunoliposomes for the single patient.

6 CONCLUSION

One of the primary aims of this thesis was to develop and characterize an intracranial animal model of human glioblastoma multiforme. Cells of the human glioblastoma multiforme line U-87 MG were inoculated into the striatum of immunodeficient nude mice and approximately 3-4 weeks after cancer cell implantation tumor growth manifested as progressive loss of weight in two thirds of the animals. The brains of two mice were sectioned and investigated histologically, revealing extensive growth and local invasion of the developed tumors. Furthermore, the intratumoral accumulation of peroxidase injected intraperitoneally and mouse albumin was investigated as a measure of vascular permeability within the tumor. DAB staining demonstrated some diffuse peroxidase activity in the central area of the tumor, neither observed in normal brain tissue nor in the tumor tissue of the mouse that had not received any exogenous peroxidase. Accordingly, some diffuse accumulation of mouse albumin could also be observed in the tumor area compared to normal brain tissue. In summary, the intracranial U-87 MG tumor xenograft model recapitulates important features of human glioblastoma multiforme, such as aggressive growth, local invasion, and probably also some degree of vascular leakiness. Further investigations might aid in characterizing the exact tumor compartment where accumulation occurs and the extent of vascular permeability.

Another aim was to develop a protocol for preparation of immunoliposomes, based on the micelle post insertion technique. The protocol was used for preparation of immunoliposomes conjugated with the EGFR-antibody Erbitux® for targeting U-87 MG cells and conjugated with VCAM-1 antibody for targeting murine brain endothelial cells. Erbitux®-liposomes demonstrated significant cellular binding and uptake by the U-87 MG cells in contrast to unconjugated liposomes. However, no uptake of anti-VCAM-1 liposomes by TNF-α activated cells of the murine brain endothelial line, bEnd.3, could be detected. Immunocytochemical investigation had confirmed the expression of VCAM-1 by TNF-α treated bEnd.3 cells. Therefore, the cause of insufficient liposomal binding to the cells might be the much lower conjugation achieved for VCAM-1 antibody compared to Erbitux®. Optimizing coupling conditions and antibody concentration may result in a higher amount of conjugated VCAM-1 antibody and specific cellular uptake of anti-VCAM-1-immunoliposomes.

Furthermore, methods for assessing the tissue distribution of fluorescent liposomes in vivo were investigated. Fluorescence microscopy of tissue sections was hampered by a high background signal and fluorescent liposomes could only be detected in the liver and the spleen, in a pattern resembling the macrophage distribution within these organs. Fluorescence spectroscopy of tissue homogenates yielded promising results, however due to time constraints data have only been obtained for some tissues. After further optimization and validation of these methods, it would be interesting to explore the in vivo characteristics of the Erbitux®-liposomes in the established U-87 MG tumor xenograft model, perhaps along with liposomes targeting the tumor endothelial cells via another marker than VCAM-1.

7 REFERENCES

1. CBTRUS. CBTRUS statistical report: Primary brain and central nervous system tumors diagnosed in the united states in 2004-2007. Hinsdale, IL: Central Brain Tumor Registry of the United States; 2011.
2. CBTRUS. CBTRUS statistical report: Primary brain and central nervous system tumors diagnosed in the united states in 2004-2006. website: www.cbtrus.org. Source: Central Brain Tumor Registry of the United States, Hinsdale, IL.; 2010.
3. Stupp R, Mason WP, van den Bent MJ, Weller M, Fisher B, Taphoorn MJ, et al. Radiotherapy plus concomitant and adjuvant temozolomide for glioblastoma. N Engl J Med. 2005 Mar 10;352(10):987-96.
4. Louis DN, Ohgaki H, Wiestler OD, Cavenee WK. WHO classification of tumours of the central nervous system. 4th ed. Louis DN, Ohgaki H, Wiestler OD, Cavenee WK, editors. Lyon, France: International Agency for Research on Cancer (IARC); 2007.
5. Wen PY, Kesari S. Malignant gliomas in adults. N Engl J Med. 2008 Jul 31;359(5):492-507.
6. Van Meir EG, Hadjipanayis CG, Norden AD, Shu HK, Wen PY, Olson JJ. Exciting new advances in neuro-oncology: The avenue to a cure for malignant glioma. CA Cancer J Clin. 2010 May-Jun;60(3):166-93.
7. Sathornsumetee S, Rich JN. Designer therapies for glioblastoma multiforme. Ann N Y Acad Sci. 2008 Oct;1142:108-32.
8. Gabizon AA, Shmeeda H, Zalipsky S. Pros and cons of the liposome platform in cancer drug targeting. J Liposome Res. 2006;16(3):175-83.
9. Chan LS, Daruwalla J, Christophi C. Selective targeting of the tumour vasculature. ANZ J Surg. 2008 Nov;78(11):955-67.
10. Chi AS, Sorensen AG, Jain RK, Batchelor TT. Angiogenesis as a therapeutic target in malignant gliomas. Oncologist. 2009 Jun;14(6):621-36.
11. Siemann DW, Horsman MR. Vascular targeted therapies in oncology. Cell Tissue Res. 2009 Jan;335(1):241-8.
12. Lammers T, Hennink WE, Storm G. Tumour-targeted nanomedicines: Principles and practice. Br J Cancer. 2008 Aug 5;99(3):392-7.
13. Sapra P, Allen TM. Ligand-targeted liposomal anticancer drugs. Prog Lipid Res. 2003 Sep;42(5):439-62.
14. Pastorino F, Brignole C, Di Paolo D, Nico B, Pezzolo A, Marimpietri D, et al. Targeting liposomal chemotherapy via both tumor cell-specific and tumor vasculature-specific ligands potentiates therapeutic efficacy. Cancer Res. 2006 Oct 15;66(20):10073-82.
15. Saul JM, Annapragada AV, Bellamkonda RV. A dual-ligand approach for enhancing targeting selectivity of therapeutic nanocarriers. J Control Release. 2006 Sep 12;114(3):277-87.
16. Kamps JAAM, Scherphof GL. Liposomes in biological systems. In: Torchilin VP, Weissig V, editors. Liposomes. 2nd ed. New York, NY, USA: Oxford University Press; 2003. p. 267-88.
17. Mui B, Chow L, Hope MJ. Extrusion technique to generate liposomes of defined size. In: Düzgünes N, editor. Methods in Enzymology Vol. 367 Liposomes Part A. 1st ed. San Diego, CA: Elsevier Academic Press; 2003. p. 3-14.
18. Ishida T, Iden DL, Allen TM. A combinatorial approach to producing sterically stabilized (stealth) immunoliposomal drugs. FEBS Lett. 1999 Oct 22;460(1):129-33.
19. CBTRUS. CBTRUS statistical report: Primary brain tumors in the united states, 2000-2004. Hinsdale, IL: Central Brain Tumor Registry of the United States; 2008.

20. Cancer incidence in five continents, volume IX. Curado MP, Edwards B, Shin HR, et al, editors. Lyon, France: IARC Scientific Publications No. 160; 2007.
21. Ohgaki H. Epidemiology of brain tumors. In: Verma M, editor. Methods of Molecular Biology, Cancer Epidemiology. vol. 472 ed. Totowa, NJ: Humana Press; 2009. p. 323-242.
22. Fisher JL, Schwartzbaum JA, Wrensch M, Wiemels JL. Epidemiology of brain tumors. Neurol Clin. 2007 Nov;25(4):867,90, vii.
23. Bondy ML, Scheurer ME, Malmer B, Barnholtz-Sloan JS, Davis FG, Il'yasova D, et al. Brain tumor epidemiology: Consensus from the brain tumor epidemiology consortium. Cancer. 2008 Oct 1;113(7 Suppl):1953-68.
24. Wrensch M, Minn Y, Chew T, Bondy M, Berger MS. Epidemiology of primary brain tumors: Current concepts and review of the literature. Neuro Oncol. 2002 Oct;4(4):278-99.
25. Ohgaki H, Kleihues P. Genetic pathways to primary and secondary glioblastoma. Am J Pathol. 2007 May;170(5):1445-53.
26. Furnari FB, Fenton T, Bachoo RM, Mukasa A, Stommel JM, Stegh A, et al. Malignant astrocytic glioma: Genetics, biology, and paths to treatment. Genes Dev. 2007 Nov 1;21(21):2683-710.
27. Ohgaki H, Kleihues P. Population-based studies on incidence, survival rates, and genetic alterations in astrocytic and oligodendroglial gliomas. J Neuropathol Exp Neurol. 2005 Jun;64(6):479-89.
28. Stiles CD, Rowitch DH. Glioma stem cells: A midterm exam. Neuron. 2008 Jun 26;58(6):832-46.
29. Das S, Srikanth M, Kessler JA. Cancer stem cells and glioma. Nat Clin Pract Neurol. 2008 Aug;4(8):427-35.
30. Folkman J. Angiogenesis. Annu Rev Med. 2006;57:1-18.
31. Jain RK, di Tomaso E, Duda DG, Loeffler JS, Sorensen AG, Batchelor TT. Angiogenesis in brain tumours. Nat Rev Neurosci. 2007 Aug;8(8):610-22.
32. Fischer I, Gagner JP, Law M, Newcomb EW, Zagzag D. Angiogenesis in gliomas: Biology and molecular pathophysiology. Brain Pathol. 2005 Oct;15(4):297-310.
33. Fukumura D, Jain RK. Tumor microvasculature and microenvironment: Targets for anti-angiogenesis and normalization. Microvasc Res. 2007 Sep-Nov;74(2-3):72-84.
34. Stupp R, Hegi ME, Gilbert MR, Chakravarti A. Chemoradiotherapy in malignant glioma: Standard of care and future directions. J Clin Oncol. 2007 Sep 10;25(26):4127-36.
35. Wen PY, Brandes AA. Treatment of recurrent high-grade gliomas. Curr Opin Neurol. 2009 Dec;22(6):657-64.
36. Cohen MH, Shen YL, Keegan P, Pazdur R. FDA drug approval summary: Bevacizumab (avastin) as treatment of recurrent glioblastoma multiforme. Oncologist. 2009 Nov;14(11):1131-8.
37. Strebhardt K, Ullrich A. Paul ehrlich's magic bullet concept: 100 years of progress. Nat Rev Cancer. 2008 Jun;8(6):473-80.
38. Thorpe PE. Vascular targeting agents as cancer therapeutics. Clin Cancer Res. 2004 Jan 15;10(2):415-27.
39. Simone E, Ding BS, Muzykantov V. Targeted delivery of therapeutics to endothelium. Cell Tissue Res. 2009 Jan;335(1):283-300.
40. Cavaliere R, Wen PY, Schiff D. Novel therapies for malignant gliomas. Neurol Clin. 2007 Nov;25(4):1141,71, x.
41. Huang TT, Sarkaria SM, Cloughesy TF, Mischel PS. Targeted therapy for malignant glioma patients: Lessons learned and the road ahead. Neurotherapeutics. 2009 Jul;6(3):500-12.
42. Adams GP, Weiner LM. Monoclonal antibody therapy of cancer. Nat Biotechnol. 2005 Sep;23(9):1147-57.

43. Chirasani SR, Markovic DS, Synowitz M, Eichler SA, Wisniewski P, Kaminska B, et al. Transferrin-receptor-mediated iron accumulation controls proliferation and glutamate release in glioma cells. J Mol Med. 2009 Feb;87(2):153-67.
44. Kawakami M, Kawakami K, Puri RK. Interleukin-4-pseudomonas exotoxin chimeric fusion protein for malignant glioma therapy. J Neurooncol. 2003 Oct;65(1):15-25.
45. Husain SR, Puri RK. Interleukin-13 receptor-directed cytotoxin for malignant glioma therapy: From bench to bedside. J Neurooncol. 2003 Oct;65(1):37-48.
46. Weaver M, Laske DW. Transferrin receptor ligand-targeted toxin conjugate (tf-CRM107) for therapy of malignant gliomas. J Neurooncol. 2003 Oct;65(1):3-13.
47. Weber FW, Floeth F, Asher A, Bucholz R, Berger M, Prados M, et al. Local convection enhanced delivery of IL4-pseudomonas exotoxin (NBI-3001) for treatment of patients with recurrent malignant glioma. Acta Neurochir Suppl. 2003;88:93-103.
48. Kunwar S, Prados MD, Chang SM, Berger MS, Lang FF, Piepmeier JM, et al. Direct intracerebral delivery of cintredekin besudotox (IL13-PE38QQR) in recurrent malignant glioma: A report by the cintredekin besudotox intraparenchymal study group. J Clin Oncol. 2007 Mar 1;25(7):837-44.
49. Bidros DS, Vogelbaum MA. Novel drug delivery strategies in neuro-oncology. Neurotherapeutics. 2009 Jul;6(3):539-46.
50. Laske DW, Youle RJ, Oldfield EH. Tumor regression with regional distribution of the targeted toxin TF-CRM107 in patients with malignant brain tumors. Nat Med. 1997 Dec;3(12):1362-8.
51. Rand RW, Kreitman RJ, Patronas N, Varricchio F, Pastan I, Puri RK. Intratumoral administration of recombinant circularly permuted interleukin-4-pseudomonas exotoxin in patients with high-grade glioma. Clin Cancer Res. 2000 Jun;6(6):2157-65.
52. Weber F, Asher A, Bucholz R, Berger M, Prados M, Chang S, et al. Safety, tolerability, and tumor response of IL4-pseudomonas exotoxin (NBI-3001) in patients with recurrent malignant glioma. J Neurooncol. 2003 Aug-Sep;64(1-2):125-37.
53. Drummond DC, Meyer O, Hong K, Kirpotin DB, Papahadjopoulos D. Optimizing liposomes for delivery of chemotherapeutic agents to solid tumors. Pharmacol Rev. 1999 Dec;51(4):691-743.
54. Sharma US, Sharma A, Chau RI, Straubinger RM. Liposome-mediated therapy of intracranial brain tumors in a rat model. Pharm Res. 1997 Aug;14(8):992-8.
55. Hau P, Fabel K, Baumgart U, Rummele P, Grauer O, Bock A, et al. Pegylated liposomal doxorubicin-efficacy in patients with recurrent high-grade glioma. Cancer. 2004 Mar 15;100(6):1199-207.
56. Fabel K, Dietrich J, Hau P, Wismeth C, Winner B, Przywara S, et al. Long-term stabilization in patients with malignant glioma after treatment with liposomal doxorubicin. Cancer. 2001 Oct 1;92(7):1936-42.
57. Maeda H. The enhanced permeability and retention (EPR) effect in tumor vasculature: The key role of tumor-selective macromolecular drug targeting. Adv Enzyme Regul. 2001;41:189-207.
58. Madhankumar AB, Slagle-Webb B, Wang X, Yang QX, Antonetti DA, Miller PA, et al. Efficacy of interleukin-13 receptor-targeted liposomal doxorubicin in the intracranial brain tumor model. Mol Cancer Ther. 2009 Mar;8(3):648-54.
59. Mamot C, Drummond DC, Noble CO, Kallab V, Guo Z, Hong K, et al. Epidermal growth factor receptor-targeted immunoliposomes significantly enhance the efficacy of multiple anticancer drugs in vivo. Cancer Res. 2005 Dec 15;65(24):11631-8.
60. Gupta B, Torchilin VP. Monoclonal antibody 2C5-modified doxorubicin-loaded liposomes with significantly enhanced therapeutic activity against intracranial human brain U-87 MG tumor xenografts in nude mice. Cancer Immunol Immunother. 2007 Aug;56(8):1215-23.

61. Norden AD, Drappatz J, Wen PY. Novel anti-angiogenic therapies for malignant gliomas. Lancet Neurol. 2008 Dec;7(12):1152-60.
62. Hinnen P, Eskens FA. Vascular disrupting agents in clinical development. Br J Cancer. 2007 Apr 23;96(8):1159-65.
63. Alessi P, Ebbinghaus C, Neri D. Molecular targeting of angiogenesis. Biochim Biophys Acta. 2004 Mar 4;1654(1):39-49.
64. Ahlskog J, Paganelli G, Neri D. Vascular tumor targeting. Q J Nucl Med Mol Imaging. 2006 Dec;50(4):296-309.
65. Kerbel R, Folkman J. Clinical translation of angiogenesis inhibitors. Nat Rev Cancer. 2002 Oct;2(10):727-39.
66. Tozer GM, Kanthou C, Baguley BC. Disrupting tumour blood vessels. Nat Rev Cancer. 2005 Jun;5(6):423-35.
67. Wedge SR, Kendrew J, Hennequin LF, Valentine PJ, Barry ST, Brave SR, et al. AZD2171: A highly potent, orally bioavailable, vascular endothelial growth factor receptor-2 tyrosine kinase inhibitor for the treatment of cancer. Cancer Res. 2005 May 15;65(10):4389-400.
68. Mathieu V, De Neve N, Le Mercier M, Dewelle J, Gaussin JF, Dehoux M, et al. Combining bevacizumab with temozolomide increases the antitumor efficacy of temozolomide in a human glioblastoma orthotopic xenograft model. Neoplasia. 2008 Dec;10(12):1383-92.
69. Vredenburgh JJ, Desjardins A, Herndon JE,2nd, Marcello J, Reardon DA, Quinn JA, et al. Bevacizumab plus irinotecan in recurrent glioblastoma multiforme. J Clin Oncol. 2007 Oct 20;25(30):4722-9.
70. Batchelor TT, Sorensen AG, di Tomaso E, Zhang WT, Duda DG, Cohen KS, et al. AZD2171, a pan-VEGF receptor tyrosine kinase inhibitor, normalizes tumor vasculature and alleviates edema in glioblastoma patients. Cancer Cell. 2007 Jan;11(1):83-95.
71. Jain RK. Normalizing tumor vasculature with anti-angiogenic therapy: A new paradigm for combination therapy. Nat Med. 2001 Sep;7(9):987-9.
72. Jain RK. Normalization of tumor vasculature: An emerging concept in antiangiogenic therapy. Science. 2005 Jan 7;307(5706):58-62.
73. Winkler F, Kozin SV, Tong RT, Chae SS, Booth MF, Garkavtsev I, et al. Kinetics of vascular normalization by VEGFR2 blockade governs brain tumor response to radiation: Role of oxygenation, angiopoietin-1, and matrix metalloproteinases. Cancer Cell. 2004 Dec;6(6):553-63.
74. Baguley BC, Ching LM. DMXAA: An antivascular agent with multiple host responses. Int J Radiat Oncol Biol Phys. 2002 Dec 1;54(5):1503-11.
75. Yamamoto M, Sawaya R, Mohanam S, Rao VH, Bruner JM, Nicolson GL, et al. Expression and localization of urokinase-type plasminogen activator receptor in human gliomas. Cancer Res. 1994 Sep 15;54(18):5016-20.
76. Hsu AR, Cai W, Veeravagu A, Mohamedali KA, Chen K, Kim S, et al. Multimodality molecular imaging of glioblastoma growth inhibition with vasculature-targeting fusion toxin VEGF121/rGel. J Nucl Med. 2007 Mar;48(3):445-54.
77. Ran S, Gao B, Duffy S, Watkins L, Rote N, Thorpe PE. Infarction of solid hodgkin's tumors in mice by antibody-directed targeting of tissue factor to tumor vasculature. Cancer Res. 1998 Oct 15;58(20):4646-53.
78. Dienst A, Grunow A, Unruh M, Rabausch B, Nor JE, Fries JW, et al. Specific occlusion of murine and human tumor vasculature by VCAM-1-targeted recombinant fusion proteins. J Natl Cancer Inst. 2005 May 18;97(10):733-47.

79. Gosk S, Moos T, Gottstein C, Bendas G. VCAM-1 directed immunoliposomes selectively target tumor vasculature in vivo. Biochim Biophys Acta. 2008 Apr;1778(4):854-63.
80. Arap W, Pasqualini R, Ruoslahti E. Cancer treatment by targeted drug delivery to tumor vasculature in a mouse model. Science. 1998 Jan 16;279(5349):377-80.
81. Kim JW, Lee HS. Tumor targeting by doxorubicin-RGD-4C peptide conjugate in an orthotopic mouse hepatoma model. Int J Mol Med. 2004 Oct;14(4):529-35.
82. Xiong XB, Huang Y, Lu WL, Zhang X, Zhang H, Nagai T, et al. Intracellular delivery of doxorubicin with RGD-modified sterically stabilized liposomes for an improved antitumor efficacy: In vitro and in vivo. J Pharm Sci. 2005 Aug;94(8):1782-93.
83. Xiong XB, Huang Y, Lu WL, Zhang H, Zhang X, Zhang Q. Enhanced intracellular uptake of sterically stabilized liposomal doxorubicin in vitro resulting in improved antitumor activity in vivo. Pharm Res. 2005 Jun;22(6):933-9.
84. Xiong XB, Huang Y, Lu WL, Zhang X, Zhang H, Nagai T, et al. Enhanced intracellular delivery and improved antitumor efficacy of doxorubicin by sterically stabilized liposomes modified with a synthetic RGD mimetic. J Control Release. 2005 Oct 3;107(2):262-75.
85. Holig P, Bach M, Volkel T, Nahde T, Hoffmann S, Muller R, et al. Novel RGD lipopeptides for the targeting of liposomes to integrin-expressing endothelial and melanoma cells. Protein Eng Des Sel. 2004 May;17(5):433-41.
86. Pastorino F, Brignole C, Marimpietri D, Cilli M, Gambini C, Ribatti D, et al. Vascular damage and anti-angiogenic effects of tumor vessel-targeted liposomal chemotherapy. Cancer Res. 2003 Nov 1;63(21):7400-9.
87. Garde SV, Forte AJ, Ge M, Lepekhin EA, Panchal CJ, Rabbani SA, et al. Binding and internalization of NGR-peptide-targeted liposomal doxorubicin (TVT-DOX) in CD13-expressing cells and its antitumor effects. Anticancer Drugs. 2007 Nov;18(10):1189-200.
88. Matsuno F, Haruta Y, Kondo M, Tsai H, Barcos M, Seon BK. Induction of lasting complete regression of preformed distinct solid tumors by targeting the tumor vasculature using two new anti-endoglin monoclonal antibodies. Clin Cancer Res. 1999 Feb;5(2):371-82.
89. Seon BK, Matsuno F, Haruta Y, Kondo M, Barcos M. Long-lasting complete inhibition of human solid tumors in SCID mice by targeting endothelial cells of tumor vasculature with antihuman endoglin immunotoxin. Clin Cancer Res. 1997 Jul;3(7):1031-44.
90. Takahashi N, Haba A, Matsuno F, Seon BK. Antiangiogenic therapy of established tumors in human skin/severe combined immunodeficiency mouse chimeras by anti-endoglin (CD105) monoclonal antibodies, and synergy between anti-endoglin antibody and cyclophosphamide. Cancer Res. 2001 Nov 1;61(21):7846-54.
91. Arora N, Masood R, Zheng T, Cai J, Smith DL, Gill PS. Vascular endothelial growth factor chimeric toxin is highly active against endothelial cells. Cancer Res. 1999 Jan 1;59(1):183-8.
92. Wild R, Dhanabal M, Olson TA, Ramakrishnan S. Inhibition of angiogenesis and tumour growth by VEGF121-toxin conjugate: Differential effect on proliferating endothelial cells. Br J Cancer. 2000 Oct;83(8):1077-83.
93. Olson TA, Mohanraj D, Roy S, Ramakrishnan S. Targeting the tumor vasculature: Inhibition of tumor growth by a vascular endothelial growth factor-toxin conjugate. Int J Cancer. 1997 Dec 10;73(6):865-70.
94. Veenendaal LM, Jin H, Ran S, Cheung L, Navone N, Marks JW, et al. In vitro and in vivo studies of a VEGF121/rGelonin chimeric fusion toxin targeting the neovasculature of solid tumors. Proc Natl Acad Sci U S A. 2002 Jun 11;99(12):7866-71.

95. Mohamedali KA, Kedar D, Sweeney P, Kamat A, Davis DW, Eve BY, et al. The vascular-targeting fusion toxin VEGF121/rGel inhibits the growth of orthotopic human bladder carcinoma tumors. Neoplasia. 2005 Oct;7(10):912-20.
96. Nilsson F, Kosmehl H, Zardi L, Neri D. Targeted delivery of tissue factor to the ED-B domain of fibronectin, a marker of angiogenesis, mediates the infarction of solid tumors in mice. Cancer Res. 2001 Jan 15;61(2):711-6.
97. Carnemolla B, Borsi L, Balza E, Castellani P, Meazza R, Berndt A, et al. Enhancement of the antitumor properties of interleukin-2 by its targeted delivery to the tumor blood vessel extracellular matrix. Blood. 2002 Mar 1;99(5):1659-65.
98. Halin C, Rondini S, Nilsson F, Berndt A, Kosmehl H, Zardi L, et al. Enhancement of the antitumor activity of interleukin-12 by targeted delivery to neovasculature. Nat Biotechnol. 2002 Mar;20(3):264-9.
99. Borsi L, Balza E, Carnemolla B, Sassi F, Castellani P, Berndt A, et al. Selective targeted delivery of TNFalpha to tumor blood vessels. Blood. 2003 Dec 15;102(13):4384-92.
100. Marty C, Odermatt B, Schott H, Neri D, Ballmer-Hofer K, Klemenz R, et al. Cytotoxic targeting of F9 teratocarcinoma tumours with anti-ED-B fibronectin scFv antibody modified liposomes. Br J Cancer. 2002 Jul 1;87(1):106-12.
101. Lasch J, Weissig V, Brandl M. Preparation of liposomes. In: Torchilin VP, Weissig V, editors. Liposomes. 2nd ed. New York, NY, USA: Oxford University Press; 2003. p. 3-30.
102. Senior J, Crawley JC, Gregoriadis G. Tissue distribution of liposomes exhibiting long half-lives in the circulation after intravenous injection. Biochim Biophys Acta. 1985 Mar 29;839(1):1-8.
103. Allen TM, Hansen C, Martin F, Redemann C, Yau-Young A. Liposomes containing synthetic lipid derivatives of poly(ethylene glycol) show prolonged circulation half-lives in vivo. Biochim Biophys Acta. 1991 Jul 1;1066(1):29-36.
104. Allen TM. Liposomes. opportunities in drug delivery. Drugs. 1997;54 Suppl 4:8-14.
105. Liu D, Mori A, Huang L. Role of liposome size and RES blockade in controlling biodistribution and tumor uptake of GM1-containing liposomes. Biochim Biophys Acta. 1992 Feb 17;1104(1):95-101.
106. Litzinger DC, Buiting AM, van Rooijen N, Huang L. Effect of liposome size on the circulation time and intraorgan distribution of amphipathic poly(ethylene glycol)-containing liposomes. Biochim Biophys Acta. 1994 Feb 23;1190(1):99-107.
107. Hansen CB, Kao GY, Moase EH, Zalipsky S, Allen TM. Attachment of antibodies to sterically stabilized liposomes: Evaluation, comparison and optimization of coupling procedures. Biochim Biophys Acta. 1995 Nov 1;1239(2):133-44.
108. Klibanov AL, Maruyama K, Beckerleg AM, Torchilin VP, Huang L. Activity of amphipathic poly(ethylene glycol) 5000 to prolong the circulation time of liposomes depends on the liposome size and is unfavorable for immunoliposome binding to target. Biochim Biophys Acta. 1991 Feb 25;1062(2):142-8.
109. Park YS. Tumor-directed targeting of liposomes. Biosci Rep. 2002 Apr;22(2):267-81.
110. Park JW, Kirpotin DB, Hong K, Shalaby R, Shao Y, Nielsen UB, et al. Tumor targeting using anti-her2 immunoliposomes. J Control Release. 2001 Jul 6;74(1-3):95-113.
111. Harding JA, Engbers CM, Newman MS, Goldstein NI, Zalipsky S. Immunogenicity and pharmacokinetic attributes of poly(ethylene glycol)-grafted immunoliposomes. Biochim Biophys Acta. 1997 Jul 25;1327(2):181-92.
112. Maruyama K. PEG-immunoliposome. Biosci Rep. 2002 Apr;22(2):251-66.

113. Maruyama K, Takizawa T, Yuda T, Kennel SJ, Huang L, Iwatsuru M. Targetability of novel immunoliposomes modified with amphipathic poly(ethylene glycol)s conjugated at their distal terminals to monoclonal antibodies. Biochim Biophys Acta. 1995 Mar 8;1234(1):74-80.
114. Allen TM, Brandeis E, Hansen CB, Kao GY, Zalipsky S. A new strategy for attachment of antibodies to sterically stabilized liposomes resulting in efficient targeting to cancer cells. Biochim Biophys Acta. 1995 Jul 26;1237(2):99-108.
115. Zalipsky S, Puntambekar B, Boulikas P, Engbers CM, Woodle MC. Peptide attachment to extremities of liposomal surface grafted PEG chains: Preparation of the long-circulating form of laminin pentapeptide, YIGSR. Bioconjug Chem. 1995 Nov-Dec;6(6):705-8.
116. Zalipsky S, Brandeis E, Newman MS, Woodle MC. Long circulating, cationic liposomes containing amino-PEG-phosphatidylethanolamine. FEBS Lett. 1994 Oct 10;353(1):71-4.
117. Zalipsky S. Synthesis of an end-group functionalized polyethylene glycol-lipid conjugate for preparation of polymer-grafted liposomes. Bioconjug Chem. 1993 Jul-Aug;4(4):296-9.
118. Park JW, Hong K, Kirpotin DB, Papahadjopoulos D, Benz CC. Immunoliposomes for cancer treatment. Adv Pharmacol. 1997;40:399-435.
119. Hobbs SK, Monsky WL, Yuan F, Roberts WG, Griffith L, Torchilin VP, et al. Regulation of transport pathways in tumor vessels: Role of tumor type and microenvironment. Proc Natl Acad Sci U S A. 1998 Apr 14;95(8):4607-12.
120. Chua SL, Rosenthal MA, Wong SS, Ashley DM, Woods AM, Dowling A, et al. Phase 2 study of temozolomide and caelyx in patients with recurrent glioblastoma multiforme. Neuro Oncol. 2004 Jan;6(1):38-43.
121. Gabizon A, Shmeeda H, Barenholz Y. Pharmacokinetics of pegylated liposomal doxorubicin: Review of animal and human studies. Clin Pharmacokinet. 2003;42(5):419-36.
122. Zandi R, Larsen AB, Andersen P, Stockhausen MT, Poulsen HS. Mechanisms for oncogenic activation of the epidermal growth factor receptor. Cell Signal. 2007 Oct;19(10):2013-23.
123. Heimberger AB, Hlatky R, Suki D, Yang D, Weinberg J, Gilbert M, et al. Prognostic effect of epidermal growth factor receptor and EGFRvIII in glioblastoma multiforme patients. Clin Cancer Res. 2005 Feb 15;11(4):1462-6.
124. Hatanpaa KJ, Burma S, Zhao D, Habib AA. Epidermal growth factor receptor in glioma: Signal transduction, neuropathology, imaging, and radioresistance. Neoplasia. 2010 Sep;12(9):675-84.
125. Vincenzi B, Zoccoli A, Pantano F, Venditti O, Galluzzo S. Cetuximab: From bench to bedside. Curr Cancer Drug Targets. 2010 Feb;10(1):80-95.
126. Loew S, Schmidt U, Unterberg A, Halatsch ME. The epidermal growth factor receptor as a therapeutic target in glioblastoma multiforme and other malignant neoplasms. Anticancer Agents Med Chem. 2009 Jul;9(6):703-15.
127. Fan Z, Lu Y, Wu X, Mendelsohn J. Antibody-induced epidermal growth factor receptor dimerization mediates inhibition of autocrine proliferation of A431 squamous carcinoma cells. J Biol Chem. 1994 Nov 4;269(44):27595-602.
128. Mamot C, Drummond DC, Greiser U, Hong K, Kirpotin DB, Marks JD, et al. Epidermal growth factor receptor (EGFR)-targeted immunoliposomes mediate specific and efficient drug delivery to EGFR- and EGFRvIII-overexpressing tumor cells. Cancer Res. 2003 Jun 15;63(12):3154-61.
129. Pan X, Wu G, Yang W, Barth RF, Tjarks W, Lee RJ. Synthesis of cetuximab-immunoliposomes via a cholesterol-based membrane anchor for targeting of EGFR. Bioconjug Chem. 2007 Jan-Feb;18(1):101-8.

130. Mamot C, Ritschard R, Kung W, Park JW, Herrmann R, Rochlitz CF. EGFR-targeted immunoliposomes derived from the monoclonal antibody EMD72000 mediate specific and efficient drug delivery to a variety of colorectal cancer cells. J Drug Target. 2006 May;14(4):215-23.
131. Pan X, Lee RJ. Construction of anti-EGFR immunoliposomes via folate-folate binding protein affinity. Int J Pharm. 2007 May 24;336(2):276-83.
132. Drummond DC, Noble CO, Guo Z, Hayes ME, Connolly-Ingram C, Gabriel BS, et al. Development of a highly stable and targetable nanoliposomal formulation of topotecan. J Control Release. 2010 Jan 4;141(1):13-21.
133. Castermans K, Griffioen AW. Tumor blood vessels, a difficult hurdle for infiltrating leukocytes. Biochim Biophys Acta. 2007 Dec;1776(2):160-74.
134. Ricard I, Payet MD, Dupuis G. VCAM-1 is internalized by a clathrin-related pathway in human endothelial cells but its alpha 4 beta 1 integrin counter-receptor remains associated with the plasma membrane in human T lymphocytes. Eur J Immunol. 1998 May;28(5):1708-18.
135. Kuzu I, Bicknell R, Fletcher CD, Gatter KC. Expression of adhesion molecules on the endothelium of normal tissue vessels and vascular tumors. Lab Invest. 1993 Sep;69(3):322-8.
136. Mantovani A, Allavena P, Sica A, Balkwill F. Cancer-related inflammation. Nature. 2008 Jul 24;454(7203):436-44.
137. Osborn L, Hession C, Tizard R, Vassallo C, Luhowskyj S, Chi-Rosso G, et al. Direct expression cloning of vascular cell adhesion molecule 1, a cytokine-induced endothelial protein that binds to lymphocytes. Cell. 1989 Dec 22;59(6):1203-11.
138. Kobayashi H, Boelte KC, Lin PC. Endothelial cell adhesion molecules and cancer progression. Curr Med Chem. 2007;14(4):377-86.
139. Voinea M, Manduteanu I, Dragomir E, Capraru M, Simionescu M. Immunoliposomes directed toward VCAM-1 interact specifically with activated endothelial cells--a potential tool for specific drug delivery. Pharm Res. 2005 Nov;22(11):1906-17.
140. Maenpaa A, Kovanen PE, Paetau A, Jaaskelainen J, Timonen T. Lymphocyte adhesion molecule ligands and extracellular matrix proteins in gliomas and normal brain: Expression of VCAM-1 in gliomas. Acta Neuropathol. 1997 Sep;94(3):216-25.
141. Derksen JTP, Scherphof GL. An improved method for the covalent coupling of proteins to liposomes. Biochim Biophys Acta. 1985;841:151-5.
142. Duncan RJ, Weston PD, Wrigglesworth R. A new reagent which may be used to introduce sulfhydryl groups into proteins, and its use in the preparation of conjugates for immunoassay. Anal Biochem. 1983 Jul 1;132(1):68-73.
143. Iden DL, Allen TM. In vitro and in vivo comparison of immunoliposomes made by conventional coupling techniques with those made by a new post-insertion approach. Biochim Biophys Acta. 2001 Aug 6;1513(2):207-16.
144. Part I animal models for central nervous tumors. In: Van Meir EG, editor. CNS Cancer: Models, Markers, Prognostic Factors, Targets, and Therapeutic Approaches. 1st ed. New York, NY, USA: Humana Press; 2009. p. 3-280.
145. Ali-Osman F. Brain tumors. In: Masters JRW, Palsson B, editors. Human Cell Culture Vol II: Cancer cell lines Part 2. New York, Boston, Dordrecht, London, Moscow: Kluwer Academic Publishers; 2002. p. 167-84.
146. Ponten J, Macintyre EH. Long term culture of normal and neoplastic human glia. Acta Pathol Microbiol Scand. 1968;74(4):465-86.

147. Candolfi M, Curtin JF, Nichols WS, Muhammad AG, King GD, Pluhar GE, et al. Intracranial glioblastoma models in preclinical neuro-oncology: Neuropathological characterization and tumor progression. J Neurooncol. 2007 Nov;85(2):133-48.
148. Strojnik T, Kavalar R, Lah TT. Experimental model and immunohistochemical analyses of U87 human glioblastoma cell xenografts in immunosuppressed rat brains. Anticancer Res. 2006 Jul-Aug;26(4B):2887-900.
149. Roberts WG, Delaat J, Nagane M, Huang S, Cavenee WK, Palade GE. Host microvasculature influence on tumor vascular morphology and endothelial gene expression. Am J Pathol. 1998 Oct;153(4):1239-48.
150. Hunter RJ. Foundations of colloid science. 2nd ed. Oxford, UK: Oxford University Press; 2001.
151. Zhou M, Diwu Z, Panchuk-Voloshina N, Haugland RP. A stable nonfluorescent derivative of resorufin for the fluorometric determination of trace hydrogen peroxide: Applications in detecting the activity of phagocyte NADPH oxidase and other oxidases. Anal Biochem. 1997 Nov 15;253(2):162-8.
152. Zhou M, Zhang C, Haugland RP. Choline oxidase: A useful tool for high-throughput assays of acetylcholinesterase, phospholipase D, phosphatidylcholine-specific phospholipase C and sphingomyelinase. In: Limbach PA, Owicki JC, Raghavachari R, Tan W, editors. Advances in Nucleic Acid and Protein Analyses, Manipulation, and Sequencing. Proceedings of SPIE Volume: 3926 ed. San Jose, California: Society of Photo-optical Instrumentation Engineers, International Biomedical Optics Society; 2000. p. 166-71.
153. Lowry OH, Rosebrough NJ, Farr AL, Randall RJ. Protein measurement with the folin phenol reagent. J Biol Chem. 1951 Nov;193(1):265-75.
154. Waterborg JK. The lowry method for protein quantitation. In: Walker JM, editor. The Protein Protocols Handbook. 2nd edition ed. Totowa, New Jersey: Humana Press; 2002. p. 7-9.
155. Enoch HG, Strittmatter P. Formation and properties of 1000-A-diameter, single-bilayer phospholipid vesicles. Proc Natl Acad Sci U S A. 1979 Jan;76(1):145-9.
156. Cheng SY, Huang HJ, Nagane M, Ji XD, Wang D, Shih CC, et al. Suppression of glioblastoma angiogenicity and tumorigenicity by inhibition of endogenous expression of vascular endothelial growth factor. Proc Natl Acad Sci U S A. 1996 Aug 6;93(16):8502-7.
157. Nishikawa R, Ji XD, Harmon RC, Lazar CS, Gill GN, Cavenee WK, et al. A mutant epidermal growth factor receptor common in human glioma confers enhanced tumorigenicity. Proc Natl Acad Sci U S A. 1994 Aug 2;91(16):7727-31.
158. Mishima K, Johns TG, Luwor RB, Scott AM, Stockert E, Jungbluth AA, et al. Growth suppression of intracranial xenografted glioblastomas overexpressing mutant epidermal growth factor receptors by systemic administration of monoclonal antibody (mAb) 806, a novel monoclonal antibody directed to the receptor. Cancer Res. 2001 Jul 15;61(14):5349-54.
159. Laccabue D, Tortoreto M, Veneroni S, Perego P, Scanziani E, Zucchetti M, et al. A novel taxane active against an orthotopically growing human glioma xenograft. Cancer. 2001 Dec 15;92(12):3085-92.
160. Gambarota G, Leenders W, Maass C, Wesseling P, van der Kogel B, van Tellingen O, et al. Characterisation of tumour vasculature in mouse brain by USPIO contrast-enhanced MRI. Br J Cancer. 2008 Jun 3;98(11):1784-9.
161. Yuan F, Salehi HA, Boucher Y, Vasthare US, Tuma RF, Jain RK. Vascular permeability and microcirculation of gliomas and mammary carcinomas transplanted in rat and mouse cranial windows. Cancer Res. 1994 Sep 1;54(17):4564-8.

162. Nister M, Libermann TA, Betsholtz C, Pettersson M, Claesson-Welsh L, Heldin CH, et al. Expression of messenger RNAs for platelet-derived growth factor and transforming growth factor-alpha and their receptors in human malignant glioma cell lines. Cancer Res. 1988 Jul 15;48(14):3910-8.
163. Hahne M, Jager U, Isenmann S, Hallmann R, Vestweber D. Five tumor necrosis factor-inducible cell adhesion mechanisms on the surface of mouse endothelioma cells mediate the binding of leukocytes. J Cell Biol. 1993 May;121(3):655-64.
164. Pober JS. Activation and injury of endothelial cells by cytokines. Pathol Biol (Paris). 1998 Mar;46(3):159-63.
165. Allen TM, Mumbengegwi DR, Charrois GJ. Anti-CD19-targeted liposomal doxorubicin improves the therapeutic efficacy in murine B-cell lymphoma and ameliorates the toxicity of liposomes with varying drug release rates. Clin Cancer Res. 2005 May 1;11(9):3567-73.
166. Elbayoumi TA, Torchilin VP. Enhanced accumulation of long-circulating liposomes modified with the nucleosome-specific monoclonal antibody 2C5 in various tumours in mice: Gamma-imaging studies. Eur J Nucl Med Mol Imaging. 2006 Oct;33(10):1196-205.
167. Lukyanov AN, Elbayoumi TA, Chakilam AR, Torchilin VP. Tumor-targeted liposomes: Doxorubicin-loaded long-circulating liposomes modified with anti-cancer antibody. J Control Release. 2004 Nov 5;100(1):135-44.